

1 ***Genetic influences on the intrinsic and extrinsic functional organizations of the***
2 ***cerebral cortex***

3

4 **Running title: GWAS of cerebral cortex functions**

5

6 Bingxin Zhao^{1,2}, Tengfei Li^{3,4}, Stephen M. Smith⁵, Zirui Fan¹, Xiaochen Yang², Yilin Yang⁶,
7 Juan Shu², Di Xiong⁷, Xifeng Wang⁷, Yue Yang⁷, Tianyou Luo⁷, Ziliang Zhu⁷, Yue Shan⁷, Yujue
8 Li², Zhenyi Wu², Heping Zhang⁸, Yun Li^{7,9,10}, Jason L. Stein^{9,11}, and Hongtu Zhu^{4,7,9,10,12*}

9

10 ¹Department of Statistics and Data Science, University of Pennsylvania, Philadelphia, PA 19104, USA.

11 ²Department of Statistics, Purdue University, West Lafayette, IN 47907, USA.

12 ³Department of Radiology, University of North Carolina at Chapel Hill, Chapel Hill, NC 27599, USA.

13 ⁴Biomedical Research Imaging Center, School of Medicine, University of North Carolina at Chapel Hill,
14 Chapel Hill, NC 27599, USA.

15 ⁵Wellcome Centre for Integrative Neuroimaging, FMRIB, Nuffield Department of Clinical Neurosciences,
16 University of Oxford, Oxford, UK.

17 ⁶Department of Computer and Information Science and Electrical and Systems Engineering, School of
18 Engineering & Applied Science, University of Pennsylvania, Philadelphia, PA 19104, USA.

19 ⁷Department of Biostatistics, University of North Carolina at Chapel Hill, Chapel Hill, NC 27599, USA.

20 ⁸Department of Biostatistics, Yale University, New Haven, CT 06511, USA.

21 ⁹Department of Genetics, University of North Carolina at Chapel Hill, Chapel Hill, NC 27599, USA.

22 ¹⁰Department of Computer Science, University of North Carolina at Chapel Hill, Chapel Hill, NC 27599, USA.

23 ¹¹UNC Neuroscience Center, University of North Carolina at Chapel Hill, Chapel Hill, NC 27599, USA.

24 ¹²Department of Statistics and Operations Research, University of North Carolina at Chapel Hill, Chapel Hill,
25 NC 27599, USA.

26

27 *Corresponding author:

28 Hongtu Zhu

29 3105C McGavran-Greenberg Hall, 135 Dauer Drive, Chapel Hill, NC 27599.

30 E-mail address: htzhu@email.unc.edu Phone: (919) 966-7250

31

1 **Abstract**

2 The human cerebral cortex is a vital component of brain function, but the genetic
3 influences on cortical functional organization remain poorly understood. In this study, we
4 used a parcellation-based approach to process resting-state and task-evoked functional
5 magnetic resonance imaging (fMRI) from over 48,000 individuals in UK Biobank and ABCD
6 studies. We identified 47 loci associated with functional areas and networks at rest, 15 of
7 which also affected functional connectivity during task performance. We observed
8 patterns of heritability and locus-specific genetic effects across different brain functional
9 areas and networks. Our findings suggest that specific functional areas and networks
10 share genetic influences with cognition, mental health, and major brain disorders such as
11 Alzheimer's disease and schizophrenia. For example, the *APOE* ε4 locus strongly
12 associated with Alzheimer's disease was particularly associated with the visual cortex in
13 the secondary visual and default mode networks in both resting and task fMRI. This study
14 contributes to our understanding of the genetic determinants of cerebral cortex function
15 by analyzing biobank-scale fMRI data in high-resolution brain parcellation. Additionally, it
16 prioritizes genetically associated fMRI traits for specific brain disorders.

17

18 **Keywords:** ABCD; Brain disorders; Brain function; fMRI; GWAS; Mental health; UK
19 Biobank.

1 The human cerebral cortex is the largest part of the human brain and controls complex
2 brain functions. Based on known functional and topographic specializations at different
3 scales, the cerebral cortex of the human brain can be divided into distinct areas and
4 networks, providing insight into the brain's functional architecture^{1,2}. To define such brain
5 partitions, a few brain parcellations have been developed over the past decade³. In
6 functional magnetic resonance imaging^{4,5} (fMRI), cerebral cortex functions can be
7 evaluated by measuring functional connectivity (or correlation of blood-oxygen-level
8 dependent [BOLD] activity) among multiple cortical areas along a given parcellation. In
9 particular, resting-state fMRI captures the intrinsic functional organization of the cortex
10 without any explicit stimuli, whereas task-evoked fMRI measures extrinsic cortical
11 interaction and temporal synchrony in response to a specific task. A variety of clinical
12 applications of both task-evoked and resting-state fMRI have revealed changes in brain
13 function in multiple neurological and psychiatric disorders, such as schizophrenia^{6,7},
14 Alzheimer's disease⁸, Parkinson's disease⁹, autism spectrum disorders¹⁰, and major
15 depressive disorder (MDD)^{11,12}.

16
17 Recently, growing literature suggested that fMRI measures may have lower test re-test
18 reliability than imaging measures of brain structures^{13,14}. As a result, a large sample size
19 is particularly important in fMRI studies to generate reproducible findings^{14,15}. For
20 example, fMRI images from thousands of individuals might be needed in association
21 analysis with human behavioral traits¹⁴. Moreover, although twin studies have
22 consistently established that brain resting and task fMRI traits are moderately heritable¹⁶⁻
23²³ (for example, the heritability range of resting fMRI was (0.2,0.6) in a recent review²⁴),
24 large imaging genetic cohorts are required to identify the specific genetic variants
25 associated with the functional brain. Fortunately, a few big fMRI databases have become
26 publicly available in recent years, including the Adolescent Brain Cognitive Development²⁵
27 (ABCD) and the UK Biobank²⁶ (UKB). Particularly, the UKB imaging study aimed to collect
28 data from 100,000 subjects²⁷, providing a new opportunity for fMRI research in one large-
29 scale cohort. Using a whole brain spatial independent component analysis (ICA)²⁸⁻³⁰
30 approach in the UKB study, the narrow sense single-nucleotide polymorphism (SNP)
31 heritability of resting fMRI traits was reported to be around 10% across the entire brain
32 and higher than 30% in some functional regions³¹. A few genome-wide association studies

1 (GWAS)³¹⁻³³ have also been recently conducted on resting fMRI using these whole brain
2 ICA-based traits. The whole brain ICA is a parcellation-free dimension reduction method
3 that estimates the functional brain regions (i.e., ICA components/regions) directly from
4 the fMRI data. Although the whole brain ICA is a powerful and popular fMRI tool, it is a
5 data-driven method, which might limit its generalizability and interpretability³⁴.
6 Specifically, the whole brain ICA attempts to capture major variations in the data. As a
7 result, ICA regions typically have large sizes, limiting their ability to capture high-
8 resolution details of brain functionality. For example, an earlier study³⁰ defined 55 ICA
9 components in the UKB³⁵ dataset, most of which are distributed across multiple brain
10 areas and networks³². It may be difficult for ICA to prioritize specific brain networks and
11 regions for specific brain disorders, limiting the use of fMRI phenotypes in
12 clinical/translational research. Moreover, it might be difficult to use ICA to compare
13 intrinsic and extrinsic functional architectures, since the ICA components estimated in
14 resting and task fMRI may not be well-aligned.

15
16 To overcome these limitations, here we used a parcellation-based approach to provide
17 fine-grained details about the genetic architecture of cerebral cortex functional
18 organizations. A recently developed human brain parcellation¹, which partitioned the
19 cerebral cortex into 360 areas (referred to as the Glasser360 atlas hereafter, **Table S1** and
20 **Fig. 1A**), was used to analyze resting and task fMRI data in the UKB study. The task
21 implemented in the UKB fMRI study was an emotional processing task^{36,37}, known to
22 robustly activate the amygdala and visual systems. The Glasser360 atlas was constructed
23 using high-quality multi-modality data from the Human Connectome Project (HCP³⁸) and
24 greatly improved the neuroanatomical resolution of human cerebral cortex annotations.
25 The 360 cortical areas were grouped into 12 functional networks³⁹, including four well-
26 known sensory networks (the primary visual, secondary visual, auditory, and
27 somatomotor), four cognitive networks (the cingulo-opercular, default mode, dorsal
28 attention, and frontoparietal), the language network, and three recently identified
29 networks (the posterior multimodal, ventral multimodal, and orbito-affective) (**Fig. 1A**).
30 In addition to pairwise functional connectivity among areas, we developed a parcellation-
31 based dimension reduction procedure to generate network-level fMRI traits via a
32 combined principal component analysis (PCA) and ICA methods³¹ in a training-validation

1 design (**Fig. S1**). Briefly, area-level functional connectivity pairs within each network and
2 between each pair of networks were summarized into network-specific traits to quantify
3 the strength of functional connectivity within each network and two different networks.
4 These network-specific traits have been mapped back to the 360 cortical areas to
5 facilitate better visualization and biological interpretation (Methods). Furthermore, we
6 examined the amplitude, which was a heritable measure of brain activity⁴⁰ used in
7 previous fMRI GWAS³¹⁻³³. Together, there were 8,531 area-level traits and 1,066 network-
8 level traits for resting fMRI and 8,531 area-level traits and 919 network-level traits for
9 task fMRI. Genetic architectures were examined at both area- and network-levels for
10 brain functions using these fMRI traits. The large number of traits 1) enabled the
11 comparison between intrinsic and extrinsic functional architectures using both resting
12 and task fMRI; and 2) uncovered much more and finer detail on the genetic influences on
13 specific functional areas and networks and their genetic links with brain-related complex
14 traits and disorders. We also processed the resting fMRI data from the ABCD study as a
15 replication dataset. Most of the ICA components used in previous resting fMRI GWAS³¹⁻³³
16 overlapped with multiple Glasser360 areas and networks (**Figs. 1B and S2**). Thus, the
17 current parcellation-based study provided more details and actionable findings for future
18 clinical research. For example, we found that the *APOE* ε4 locus was particularly
19 associated with the functional connectivity of the visual cortex in the secondary visual
20 and default mode networks, prioritizing fMRI biomarkers for practical applications in
21 Alzheimer's disease research.

22

23 RESULTS

24 **Heritability of human cerebral cortex functional connectivity at rest and during a task.**
25 We examined the heritability pattern of functional connectivity traits across different
26 functional areas and networks. Using the UKB individuals of white British ancestry ($n =$
27 34,641 for resting and 32,144 for task), SNP heritability was estimated via GCTA⁴¹ for the
28 8,531 area-level within-network functional connectivity traits in both resting and task
29 fMRI. The mean heritability (h^2) was 10.4% for resting and 6.6% for task fMRI. Overall, the
30 SNP heritability of 97.9% (8,349/8,531, h^2 range = (2.4%, 27.0%)) functional connectivity
31 traits in resting fMRI and 80.8% (6,894/8,531, h^2 range = (2.9%, 24.1%)) functional
32 connectivity traits in task fMRI remained significant after adjusting for multiple

1 comparisons using the Benjamini-Hochberg procedure to control the false discovery rate
2 (FDR) at 0.05 level (**Table S2**). We also estimated the heritability of the 1,985 network-
3 level traits (1,066 for resting and 919 for task), 1049 resting fMRI traits and 893 task fMRI
4 traits were significant at the FDR 0.05 level. The mean h^2 was 32.2% for amplitude traits
5 (h^2 range = (20.8%, 46.1%)) and 12.2% for functional connectivity traits in resting fMRI (h^2
6 range = (3.3%, 32.7%)); and that was 19.6% for amplitude traits (h^2 range = (11.3%,
7 23.7%)) and 10.6% for functional connectivity traits (h^2 range = (3.4%, 24.9%)) in task fMRI
8 (**Table S3**). To better visualize the observed patterns, we mapped the area-level and
9 network-level traits back to the 360 cortical areas and created the surface maps of the
10 average heritability. Consistent with the above observations, we found that amplitude
11 traits were more heritable than functional connectivity traits ($P < 2.2 \times 10^{-16}$, Wilcoxon
12 rank test). Furthermore, among functional connectivity traits, network-level traits
13 exhibited higher heritability than area-level traits ($P < 2.2 \times 10^{-16}$, as shown in **Figs. S3** and
14 **S4A**). The higher heritability of network-level fMRI traits may suggest that our dimension
15 reduction approach reduces noise by aggregating fMRI signals or that genetics have a
16 stronger influence on broader brain networks rather than specific area pairs. In addition,
17 the average heritability of Glasser360 parcellation-based traits was higher than that of
18 the whole brain ICA-based traits³¹⁻³³ estimated from almost the same UKB resting fMRI
19 dataset (mean = 9.4% and 27.2% for functional connectivity and amplitude traits,
20 respectively, $P < 2.2 \times 10^{-16}$). The results were summarized in **Figures S4B-S4E**.

21
22 Our parcellation-based traits revealed area- and network-specific information about
23 genetic influences on the human brain. **Figures 2A** and **S5A** illustrate the heritability
24 pattern across different networks. The mean heritability was highest in the ventral
25 multimodal network in resting fMRI (mean = 20.4%). The ventral multimodal is a recently
26 identified network, consisting of four cortical areas (left/right TF and PeEc) on the ventral
27 surface of the temporal lobe³⁹. One possible function of this network is to represent
28 higher-order semantic categories³⁹. In addition, the mean heritability of task fMRI was
29 lower than that of resting fMRI in all networks except for the secondary visual network,
30 where more than half (52.32%) of connectivity traits had greater heritability in task fMRI
31 than in resting fMRI (**Fig. S5B**). This might be partly because the visual cortex is highly
32 activated when performing the emotional processing task^{36,37}. We also compared the

1 estimates of genetic variance between the resting and task fMRI. We observed a general
2 reduction in genetic variance in task fMRI ($P < 2.2 \times 10^{-16}$), and the spatial patterns of
3 genetic variance were similar to those of heritability (Figs. S6-S7). The correlation
4 between all heritability estimates for resting and task fMRI traits was 0.223, with a range
5 of 0.024 to 0.386 in most networks (Fig. S8). Overall, large-scale fMRI data indicate
6 different genetic influences in resting and task functional connectivity measurements.

7

8 In each network, the heritability pattern across functional areas was identified. For
9 example, according to physical locations, the areas of the default mode network can be
10 divided into seven clusters (Fig. S9). There is no significant correlation between the
11 physical distance of these default mode area pairs and their heritability measurements (P
12 = 0.563). In the visual cluster (including the precuneus, calcarine, and cingulate) and the
13 temporal cluster, the default mode connectivity traits were most heritable. Additionally,
14 the connectivity traits between the two clusters and the angular and frontal clusters
15 showed high heritability, indicating the high degree of genetic control of functional
16 interaction among these physically disconnected regions (Fig. 2B). In the somatomotor
17 network, the left/right 3a, 3b, and 4 areas (in the postcentral, precentral, and paracentral)
18 and the left/right 7AL and 7PC areas (in the superior parietal) form two separate
19 connectivity clusters. We found that the 3a, 3b, and 4 areas had the highest heritability
20 within the somatomotor network, while the heritability of the 7AL and 7PC areas was low.
21 In addition, the connectivity traits associated with the left OP2-3 area (in the Rolandic
22 operculum and insula) had high heritability (Fig. S10). In the cingulo-opercular network,
23 the insula-related areas (e.g., the left/right FOP5, Pol1, FOP3, FOP1, FOP4, MI, and Pol2)
24 exhibited the highest heritability. However, the heritability of the adjacent para-insular
25 area (the left/right PI, in the temporal pole and superior temporal) was low (Fig. S11). The
26 insula is a functionally diverse part of the cortex involved in multiple functions, including
27 emotion, cognition, and sensory perception^{42,43}. The insula has been found to have the
28 highest heritability in surface curvature analysis of cortical morphometry²². Additionally,
29 the connectivity traits of several specific areas showed consistently high heritability in
30 resting fMRI, including the left/right IPS1 areas (in the superior occipital) of the secondary
31 visual network and the right TE1m and left/right TE1p areas (in the inferior temporal and
32 middle temporal) of the frontoparietal network (Fig. S12). In task fMRI, we also observed

1 a few areas that had higher heritability than others, including the visual cluster, left OFC
2 (orbitofrontal complex), and left/right 25 areas (in the olfactory cortex) of the default
3 mode network (**Fig. S13**); the left/right RSC (in the middle cingulate), POS2 (in the
4 precuneus and cuneus), 7Pm (in the precuneus) areas of the frontoparietal network (**Fig.**
5 **S14**); and the middle cingulate-related areas (e.g., the left/right p24pr, a24pr, and left
6 33pr) of the cingulo-opercular network (**Fig. S15**). Furthermore, we investigated the
7 relationship between heritability estimates and the size of cortical areas. We found that
8 a greater signal-to-noise ratio in larger areas may account for some of the observed
9 differences in amplitude heritability (R-squared range = [0.03, 0.07], $P < 7.47 \times 10^{-4}$), but
10 has a weaker effect on functional connectivity heritability (R-squared range = [0, 0.02], P
11 $> 5.14 \times 10^{-3}$, **Fig. S16**). In summary, our results demonstrate the diverse genetic
12 influences on the cerebral cortex and highlight the crucial functional areas and their
13 interactions that are significantly impacted by genetic factors.

14

15 The heritability pattern was also correlated with the activation maps defined in task fMRI
16 (Shapes activation, Faces activation, and Faces-Shapes contrast)³⁰. In resting fMRI, the
17 heritability of functional connectivity traits located in task-defined activated regions was
18 lower than that of nonactivated functional connectivity traits (**Fig. 2C**, mean = 8.9% vs.
19 10.8%, $P < 2.2 \times 10^{-16}$). However, in task fMRI, activated traits had higher heritability than
20 nonactivated ones (mean = 7.4% vs. 6.3%, $P < 2.2 \times 10^{-16}$). Similar results were also
21 observed on genetic variance estimates ($P < 2.2 \times 10^{-16}$, **Fig. S6B**). These differences can
22 be partially explained by the task-related changes in brain functional activities and inter-
23 regional connectivities⁴⁴. Our findings may also be related to previous observations that
24 the correlation between two activated regions increases during task performance,
25 whereas the correlation between other regions is decreased⁴⁵. Overall, these results
26 provide insights into the genetic influences on intrinsic and extrinsic functional
27 architectures.

28

29 **Genetic loci associated with cerebral cortex functional areas and networks.**

30 GWAS was performed for the $8,531 \times 2$ within-network area-level connectivity traits in
31 resting and task fMRI using the UKB individuals of white British ancestry (Methods). The
32 LDSC intercepts⁴⁶ were close to one, suggesting no genomic inflation of test statistics due

1 to confounding factors (mean intercept = 1.0002, range = (0.987, 1.019)). At a stringent
2 significance level 2.93×10^{-12} ($5 \times 10^{-8}/8,531/2$, additionally adjusted for the number of
3 traits studied), we identified independent (linkage disequilibrium [LD] $r^2 < 0.1$) significant
4 associations in 32 genomic regions (cytogenetic bands) for resting fMRI, 9 of which were
5 also associated with task fMRI (**Fig. 3A** and **Table S4**).

6

7 Enrichment of locus-specific genetic effects was observed across different areas and
8 networks in resting fMRI. Many of the fMRI-associated genetic variants are known to
9 affect gene expressions in previously published human brain expression quantitative trait
10 loci (eQTL) datasets^{47,48}. We have highlighted the associated brain areas and networks for
11 identified genomic loci in **Figures S17-S45** and summarized these results in **Table S4**. For
12 example, most of the associations of the 2q14.1 locus were in the somatomotor network.
13 The 2q14.1 locus was also particularly associated with the right MST and right V6 areas
14 (in the middle temporal and cuneus) of the secondary visual network and a few areas
15 (e.g., the left/right 43 in the Rolandic operculum and the p24pr in the middle cingulate)
16 of the cingulo-opercular network (**Fig. S17**). **Figure S18** illustrates the genes presented at
17 this locus and shows that the index variant (and its proxy variants, LD $r^2 > 0.8$) are
18 associated with the expression of *PAX8* and *FOXD4L1* in brain tissues⁴⁷, suggesting that
19 the two genes are relevant to neuronal function. Interestingly, all associations at the
20 19q13.32 locus, which was the major genetic risk factor of the late-onset Alzheimer's
21 disease, were in the secondary visual network (such as the left LO1 and right V3CD in
22 middle occipital, left/right V3A in superior occipital, and left/right V6 in cuneus), with one
23 exception in the visual cluster of the default mode network (**Figs. 3B** and **S29-S30**). These
24 results highlight the close relationship between the 19q13.32 locus and the functional
25 connectivity measurements of the visual cortex. For task fMRI, the 10q23.33 locus was
26 mainly associated with the visual cluster of the default mode network (**Figs. S43-S44**),
27 especially the left/right 31pv areas (in the middle cingulate) (**Fig. S45**). In other genomic
28 loci (e.g., 10q26.3, 3p11.1, and 19q13.32), the associated networks in task fMRI were
29 similar to those in resting fMRI, although the number of connectivity traits surviving the
30 stringent significance level became much smaller. We examined the pairwise genetic
31 correlations between the 8,531 connectivity traits in resting and task fMRI via the cross-
32 trait LD score regression⁴⁹ (Methods). The average genetic correlation among all the 8,531

1 pairs was 0.554, 3,598 of which were significant at the FDR 5% level (**Fig. S46**, mean =
2 0.710, standard error = 0.192). Although it was more difficult to identify associated loci
3 for task fMRI, these strong genetic correlations suggest the overall similarity of the
4 genetic architecture on brain functions at rest and during a task.

5

6 Next, we performed GWAS for the 1,985 network-level traits to identify variants
7 associated with network-specific functional connectivity measurements (within each of
8 the 12 networks and between each pair of networks). At the 2.51×10^{-11} ($5 \times 10^{-8}/1,985$)
9 significance level, we identified 41 (15 additional) genomic regions for resting fMRI, 14 of
10 which were also associated with task fMRI (**Table S5**). On average, these 41 genetic
11 regions explained 13.5% of the heritability of network-level fMRI traits. Together, the
12 area- and network-level analysis identified 47 genomic regions for resting fMRI, 15 of
13 which were also associated with task fMRI (**Fig. 3A**). The whole brain ICA analysis on
14 largely the same resting fMRI dataset identified 45 associated genomic regions^{32,33} ($P <$
15 2.81×10^{-11} , $5 \times 10^{-8}/1,777$). Of the 45 regions, 31 were also identified in our study, with
16 more detailed association patterns being uncovered (**Table S6** and **Fig. S47**). For example,
17 the 19q13.32 region (index variant rs429358) had been found to be associated with the
18 amplitude traits of large ICA-defined regions spanning multiple cognitive and visual
19 networks. In the present study, as shown in **Figures 3B** and **S29-S30**, the area- and
20 network-specific fMRI traits prioritized associations with the visual cortex. Furthermore,
21 we identified 16 new loci that were associated with multiple areas and networks. For
22 example, the 12p11.22 region (index variant rs11049367) was associated with the
23 functional connectivity traits of the frontoparietal and default mode networks, especially
24 the connectivity between the right p9-46v and right TE1m areas in the frontoparietal
25 network ($P < 2.12 \times 10^{-11}$). Of the 47 fMRI-associated loci, 19 had been linked to brain
26 structural connectivity traits in a recent study of white matter microstructure using
27 diffusion MRI (dMRI)⁵⁰ (**Table S7**). A few of the 19 overlapped loci had wide genetic effects
28 on multiple white matter tracts and functional networks, such as the 16q24.2, 3p11.1,
29 16q24.2, and 15q14 (**Fig. S48**).

30

31 We aimed to replicate the identified genomic loci using independent European and non-
32 European datasets. First, we repeated GWAS on a European dataset with 8,197 subjects,

1 including European individuals in the UKB phases 4 and 5 data (up to 2023 release,
2 removed the relatives of our discovery sample) and individuals of white but non-British
3 ancestry in UKB phases 1 to 3 data. For the 266 independent ($LD\ r^2 < 0.1$) network-locus
4 associations in resting fMRI, 93 (34.9%) passed the Bonferroni significance level (1.9×10^{-4} , $0.05/266$) in this validation GWAS, and 200 (75.1%) were significant at the nominal
5 significance level (0.05). All of the 200 significant associations had concordant directions
6 in the two GWAS (Fig. S49A). Of the 47 identified genomic loci, at least one association of
7 21 loci (44.6%) passed the Bonferroni significance level and 39 (82.9%) can be validated
8 at the nominal significance level. For task fMRI, 29.8% (i.e., 17/57) network-locus
9 associations passed the nominal significance level, all of which had the same effect signs
10 in the two GWAS (Fig. S49B). The 17 associations were related to eight genomic loci, four
11 of which were significant at the Bonferroni significance level, including the 10q23.33,
12 16q24.2, 10q26.3, and 15q14.

14

15 Next, we performed GWAS on two UKB non-European validation datasets: the UKB Asian
16 (UKBA, $n = 517$) and UKB Black (UKBBL, $n = 283$). Of the 47 genomic loci, 15 (2 also in task)
17 were validated in UKBA and 12 (5 also in task) were significant in UKBBL at the nominal
18 significance level, one of them (2q13 in UKBA) survived the Bonferroni significance level
19 (Tables S4-S5). For resting fMRI, we performed further analysis using data from the ABCD
20 study. For the 266 independent ($LD\ r^2 < 0.1$) network-locus associations in resting fMRI,
21 40 (15.0%) were significant at the nominal significance level, most (37/40) had concordant
22 directions in UKB and ABCD European cohort ($n = 3,821$) (Fig. S49C). Of the 47 identified
23 genomic loci, at least one association of 16 loci (34.0%) can be validated at the nominal
24 significance level. In addition, 18 associations in 8 loci and 15 associations in 9 loci can be
25 validated in ABCD Hispanic ($n = 768$) and African American ($n = 1,257$) cohorts,
26 respectively.

27

28 Several additional analyses were performed to evaluate the robustness of our GWAS
29 results. First, we used the Yeo-7 atlas⁵¹ to group the 360 cortical areas into 7 functional
30 networks and derived 615 network-level traits (294 for resting fMRI and 321 for task fMRI)
31 using the same dimension reduction procedure as we used for the 12 functional
32 networks³⁹. The heritability estimates for these Yeo-7 network-level traits were in a

1 similar range to those based on the 12 networks (**Fig. S50**). At the stringent GWAS
2 significance level 8.13×10^{-11} ($5 \times 10^{-8}/615$, additionally adjusted for the number of Yeo-7
3 traits), we identified 28 genomic regions for resting fMRI, 23 of which overlapped with
4 the 41 regions identified by the 12 networks, and 22 overlapped with the 45 regions
5 identified by whole brain ICA analysis^{32,33} (**Fig. S51**). In task fMRI, four regions were
6 identified and all of them were also identified by the network-level traits in our main
7 analyses (**Table S8**). Second, we applied additional quality control procedures for fMRI
8 data and removed more images with potentially poor quality (492 subjects in resting fMRI
9 and 993 in the task fMRI). We rerun our heritability and GWAS analyses and found that
10 the results were consistent before and after these additional quality control steps (**Figs.**
11 **S52-S53**). Finally, we used a split-half design for our discovery GWAS sample to further
12 examine the replicability of our results. The significant genetic estimates produced by our
13 discovery GWAS were similar in the two independent half-samples for both area-level and
14 network-level traits (**Fig. S54**). Additionally, we used the first half of the sample as a
15 discovery dataset, and the second half as a replication dataset with balanced sample size
16 and homogeneous genetic background. Using the same significance level as for the full
17 discovery GWAS, we identified 17 genomic regions associated with resting fMRI, three of
18 which were associated with task fMRI. All these regions were among the 47 genomic
19 regions reported in **Figure 3A**. The genetic estimates in the two half-samples were highly
20 similar (correlation = 0.981, **Fig. S55**).
21

22 **The shared genetic influences with complex brain traits and disorders.**

23 To evaluate the shared genetic influences between brain functional organizations and
24 complex brain traits and diseases, we conducted association lookups for independent (LD
25 $r^2 < 0.1$) significant variants (and variants in LD, $r^2 \geq 0.6$) detected in the UKB white British
26 GWAS. In the NHGRI-EBI GWAS catalog⁵², our results tagged variants reported for a wide
27 range of complex traits and diseases, such as neurological disorders, neuropsychiatric
28 disorders, mental health and psychological traits, migraine, cognitive traits, educational
29 attainment, sleep, smoking/drinking, and anthropometric measurements. The top five
30 frequently tagged regions included 19q13.32 (the most frequently reported gene in prior
31 literature was *APOE*), 2q14.1 (*PAX8*), 10q23.33 (*PLCE1*), 17q21.31 (*MAPT*), and 6q16.1
32 (*FHL5*), which covered 81.66% of all tagged trait-variant associations. To explore the

1 detailed genetic overlap pattern across brain functional areas, we further took the index
2 variants of these complex traits/diseases and performed variant-specific association
3 analysis for all the 64,620 functional connectivity traits (Methods). All the loci highlighted
4 below have been replicated at the nominal significance level in the validation GWAS.
5 These results have been summarized in **Table S9**.

6
7 The rs429358 (19q13.32), one of the two variants in the *APOE* ε4 locus, is a well-known
8 risk factor for Alzheimer's disease. In this locus, we observed the shared genetic
9 influences with Alzheimer's disease in both resting and task fMRI (**Figs. 4A-B**). We further
10 applied Bayesian colocalization analysis⁵³ to test colocalization between fMRI traits and
11 Alzheimer's disease, which was defined as having a posterior probability of the shared
12 causal variant hypothesis (PPH4) > 0.8^{53,54}. Strong colocalizations between fMRI traits and
13 Alzheimer's disease were identified (PPH4 > 0.946). Furthermore, in both resting and task
14 fMRI, the secondary visual network had the strongest association with rs429358 (**Figs. 4C**
15 and **S56A**). The allele associated with increased risk for Alzheimer's disease ("C") was
16 associated with decreased functional connectivity in the visual cortex (**Fig. S57**). Visual
17 deficits were one of the first symptoms of Alzheimer's disease⁵⁵ and functional
18 connectivity deficits in the visual cortex have been reported in Alzheimer's disease^{56,57}.
19 Decreased eigenvector centrality in the visual cortex was associated with *APOE* ε4
20 carriership among normal elderly subjects⁵⁸. In addition, the risk allele at rs429358 was
21 associated with decreased default mode activity at the Bonferroni significance level in
22 variant-specific analysis (3.86×10^{-7} , $0.05/64,620/2$), with distinct patterns in resting and
23 task fMRI (**Fig. S56B**). In resting fMRI, the associations were mainly in the visual cluster
24 and the left/right 10d areas (in the superior frontal). Decreased default mode network
25 connectivity in the posterior cingulate cortex/precuneus, orbital and middle frontal
26 cortex, and inferior parietal lobe in *APOE* ε4 carriers has been consistently reported in
27 various studies across adulthood (see Section 3.3.1 and Table 2 of Foo, et al. ²⁴).
28 Regardless of *APOE* carrier status, results from previous studies are consistent in finding
29 decreased functional connectivity in the default mode network in subjects with
30 Alzheimer's disease and mild cognitive impairment, as summarized in Dennis and
31 Thompson ⁵⁹ and Badhwar, et al. ⁸. For task fMRI, most of the significant rs429358 effects
32 were on the interactions between the visual cluster and a few areas in the frontal cluster,

1 including the left/right p32 (in the medial superior frontal), a24 (in the pregenual anterior
2 cingulate cortex), and 8Ad (in the superior frontal) areas. The reduced deactivation of the
3 default mode network during tasks has been observed in different stages of Alzheimer's
4 disease⁶⁰ and normal carriers of the *APOE* ε4⁶¹. Biologically, amyloid-β (Aβ) accumulation
5 preferentially starts in several of the core regions of the default mode network, and the
6 earliest Aβ accumulation is further associated with hypoconnectivity within the default
7 mode network and between the default mode and frontoparietal networks⁶². The
8 rs429358 was also strongly associated with the secondary visual and default mode
9 networks in our analysis of the Yeo-7 networks (**Fig. S58**). Furthermore, we found the risk
10 allele at rs429358 decreased the functional connectivity of middle temporal areas in the
11 language network (e.g., the left/right TPOJ and STSdp) and the left IPO area (in the middle
12 occipital) of the dorsal attention network in task fMRI, but not in resting fMRI (**Fig. S59**).
13 We also tested the association between rs429358 and MRI traits of other imaging
14 modalities, including structural connectivity traits from dMRI⁵⁰ and regional brain
15 volumes from structural MRI (sMRI)⁶³. The fMRI traits had much stronger associations
16 (smaller *P*-values) with rs429358 than these structural traits. Together, these results
17 suggest the fMRI traits of brain functions, especially the ones from the visual cortex in the
18 secondary visual and default mode networks, might be more directly related to the
19 genetic pathways of *APOE* ε4 to Alzheimer's disease than brain morphology. These fMRI
20 traits could be used as imaging biomarkers in etiologic study of Alzheimer's disease and
21 drug development targeting *APOE* ε4.

22
23 In the 17p11.2 and 2p16.1 regions, we observed the shared genetic influences between
24 the default mode network and multiple psychiatric disorders, including schizophrenia^{64,65},
25 autism spectrum disorder⁶⁶, MDD⁶⁷, and epilepsy⁶⁸. For example, we tagged rs4273100
26 and rs1518395, which have been implicated with schizophrenia (**Fig. S60**). Rs1518395 was
27 also a risk variant for MDD and the rs2947349 in 2p16.1 was associated with epilepsy. In
28 resting fMRI, all three index variants exhibited the strongest associations with the default
29 mode network, especially the frontal cluster (**Figs. S61-S62**). In addition, we observed the
30 shared genetic influences with cognitive ability and education⁶⁹ in the 17p11.2 region and
31 with psychological traits (e.g., neuroticism⁷⁰ and subjective well-being⁷¹) in the 2p16.1
32 region, which were also mainly related to the default mode network (**Fig. S63**). In the

1 10q23.33 and 6q16.1 regions, our identified variants tagged those that have been
2 implicated with migraine^{72,73} (**Fig. S64**). These genetic effects affected multiple networks
3 and had the strongest associations in the auditory and cingulo-opercular networks (**Figs.**
4 **S65- S66**). We also tagged risk variants of brain aneurysm⁷⁴ and cerebral blood flow⁷⁵ in
5 these regions. Migraine is a heterogeneous disorder and no neuroimaging biomarker has
6 been well established in previous small sample fMRI studies⁷⁶. Our results may help
7 identify whether risk variants of migraine predispose to migraine in particular brain areas
8 or networks. Specifically, our findings suggest the genetic overlaps among migraine,
9 cerebrovascular traits, and brain functions across multiple networks, especially the
10 auditory and cingulo-opercular networks.

11

12 The shared genetic influences with cognitive ability⁶⁹, intelligence⁷⁷, and education⁶⁹ were
13 observed in the 10q26.13, 5q15, and 3p11.1 regions (**Fig. S67**). The index variants of these
14 cognitive traits were associated with a few specific functional areas in the temporal and
15 parietal lobes. For example, in the 10q26.13 locus, our tagged variant (rs2629540) was
16 associated with math ability, education⁶⁹, and cocaine dependence⁷⁸. Rs2629540 was
17 particularly associated with the precuneus-related areas in different networks, such as
18 the right PCV in the posterior multimodal network, the left/right 7Pm in the frontoparietal
19 network, and the right 31pd in the default mode network (**Fig. S68**). The precuneus is
20 involved in a variety of complex functions and responds to a wide variety of cognitive
21 processes⁷⁹. In the 5q15 region, we observed shared genetic effects with cognitive
22 performance, math ability, and education⁶⁹, most of which were related to the left/right
23 TPOJ2 areas (in the middle temporal) of the posterior multimodal network (**Fig. S69A**).
24 The *NR2F1* is well studied in the arealization of the cerebral cortex⁸⁰. In the 3p11.1 region,
25 we tagged variants associated with intelligence⁷⁷ (rs7652296, *EPHA3*). The *EPHA3* is
26 involved in axon guidance⁸¹ and the rs7652296 was mainly associated with between-
27 network connectivity of a few temporal and parietal areas (**Fig. S69B**). These findings
28 partially support the parieto-frontal integration theory of intelligence^{82,83}, uncovering the
29 genetic overlaps between cognitive functions and specific temporal and parietal
30 functional areas.

31

1 In addition, we found colocalized genetic effects with psychological traits (e.g., risk-taking
2 behaviors⁸⁴) in the 3q24 (rs2279829) and 3p12.1 (rs6762267) regions (**Fig. S70**).
3 Rs2279829 and rs6762267 were mainly related to the interactions among the
4 frontoparietal, cingulo-opercular, and default mode networks, with the strongest genetic
5 effects being on a few frontal areas (**Fig. S71**). Increasing evidence suggests the frontal
6 lobe plays an important role in risk-taking and risk behaviors⁸⁵. In summary, brain
7 functions measured in fMRI have substantial area-specific genetic overlaps with complex
8 brain traits and clinical outcomes. Uncovering the detailed genetic colocalized patterns
9 may help understand how alterations in specific brain functions lead to risk for brain
10 conditions and disorders.

11

12 **Genetic correlations with complex traits.**

13 To further explore the genetic links, we examined the genetic correlations (GC)⁴⁹ between
14 fMRI traits and 50 complex traits, most of which had genetic overplays with fMRI traits,
15 as well as additional mental health traits and major brain disorders. First, we examined
16 the genetic correlations with 4 global functional connectivity and amplitude traits (2 traits
17 for resting and 2 for task). At the FDR 5% level (4×50 tests), we found the global fMRI
18 traits were significantly associated with hypertension, neuroticism (e.g., feeling nervous
19 and worry), sleep traits, and task-taking behaviors (e.g., automobile speeding) (**Table**
20 **S10**). For example, resting functional connectivity was negatively correlated with
21 neuroticism (feeling nervous, $GC = -0.181, P < 1.14 \times 10^{-4}$) and sleep duration ($GC = -0.173,$
22 $P < 1.58 \times 10^{-4}$). Hypertension was negatively correlated with the global amplitude in task
23 fMRI ($GC = -0.282, P < 7.34 \times 10^{-6}$).

24

25 Next, we explored the spatial patterns of genetic overlaps by evaluating the genetic
26 correlations between complex traits and 8,531 functional connectivity traits. Area- and
27 network-specific genetic overlaps were widely observed in resting fMRI. For example, at
28 the FDR 5% level (8,531 tests), cognitive function⁸⁶ had genetic correlations with cognitive
29 networks (the cingulo-opercular, default mode, frontoparietal, and dorsal attention),
30 such as the right IFSa area (in the triangular part of inferior frontal) (**Fig. 5A**). Most of the
31 significant genetic correlations were negative, which suggest genetic effects predispose
32 to less resting connectivity is associated with increased intelligence. For schizophrenia⁸⁷

1 and cross-disorder⁸⁸, we found consistent positive genetic correlations with the default
2 mode network (e.g., the left/right 47s in the posterior orbital and the left/right 8BL in the
3 medial superior frontal) and negative genetic correlations with the secondary visual
4 network (e.g., the left/right LIPv in the superior parietal) (**Figs. 5B and S72**). Similarly, we
5 found neuroticism⁸⁹ (feeling nervous) had positive genetic correlations with the default
6 mode network (e.g., the right PGi in the angular) and negative genetic correlations with
7 the secondary visual network (e.g., the right FST in the middle temporal and the right
8 VMV3 in the fusiform) (**Fig. S73**).

9

10 Task fMRI provided additional insights into the genetic correlations with cognitive
11 function (**Fig. 5C**). Similar to resting fMRI, the default mode network had negative genetic
12 correlations with cognitive function. The correlations were enriched in connectivity traits
13 between the visual cluster and the frontal cluster (**Fig. S74A**). Moreover, the secondary
14 visual and somatomotor networks (e.g., the right V6 in the cuneus, the left VMV2 in the
15 lingual, the left VIP in the superior parietal, and the right OP2-3 in Rolandic operculum
16 and insula) had positive genetic correlations with cognitive function (**Fig. S74B**). In
17 summary, these results show the default mode network has negative genetic correlations
18 with cognition and positive genetic correlations with brain disorders and neuroticism. The
19 genetic correlations with cognition had opposite directions in the default mode network
20 and the secondary visual network in task fMRI, pointing to genetic influences on task-
21 specific brain activity. Patterns of other complex traits (e.g., snoring, sleep duration,
22 hypertension, general risk tolerance, and education) were summarized in the
23 **Supplementary Note** and **Figures S75-S76**. In summary, discovering genetic co-variations
24 with complex traits and diseases in specific brain areas and networks might improve our
25 understanding of how brain function is affected by genetic risk factors and aid early
26 detection and timely treatment of brain diseases.

27

28 **Gene-level analysis and biological annotations.**

29 Using GWAS summary statistics of network-level fMRI traits, MAGMA⁹⁰ detected 67
30 significant genes with 352 associations ($P < 1.34 \times 10^{-9}$, adjusted for 1,985 phenotypes).
31 The area-level traits additionally yielded 7 associated genes for resting fMRI and 1 for task
32 fMRI ($P < 1.55 \times 10^{-10}$, adjusted for $8,531 \times 2$ phenotypes, **Table 11**). Among the 75 genes,

1 30 had not been identified by the whole brain ICA analysis³² (**Fig. S77**). We performed
2 functional lookups for these fMRI-associated genes. First, nine genes (such as *SSH2* and
3 *KANSL1*) showed a high probability of being loss-of-function (LoF) intolerant⁹¹ ($pLI > 0.98$),
4 indicating extreme intolerance of LoF variation. Second, 24 (such as *FAM53B* and
5 *METTL10*) of the 67 genes were identified by a recent eQTL study of developing human
6 brain⁹², and 15 were in previously constructed transcriptional networks⁹³, such as the
7 *FAT3*, *MEF2C*, *CRHR1*, *NR2F1*, and *VRK2*, which were in the *adult neurons, synaptic*
8 *transmission, and neuron projection development* function module. Our findings showed
9 substantial overlaps with genes reported in previous studies on brain genetics. For
10 example, *CRHR1* plays an important molecular role in regulating amygdala function and
11 anxiety⁹⁴⁻⁹⁷ and was significantly associated with the functional connectivity of the
12 frontoparietal network ($P = 2.34 \times 10^{-11}$). The *MEF2C* was associated with frontoparietal,
13 default mode, and language networks in our analyses ($P < 2.25 \times 10^{-10}$) and is known to
14 cause multiple Mendelian disorders characterized by intellectual disability^{98,99}. In
15 addition, we applied FUMA¹⁰⁰ to map significant variants ($P < 2.51 \times 10^{-11}$) to genes via
16 physical position, eQTL association, and 3D chromatin (Hi-C) interaction. FUMA yielded
17 226 associated genes, 166 of which were not discovered in MAGMA (**Table S12**). For
18 example, we found associations between the default mode network and *SLC6A4*, which
19 is involved in the epigenetic mechanism of increased risk for mental illness and abnormal
20 brain function¹⁰¹⁻¹⁰⁴. In addition, 5 of the fMRI-associated genes (*CALY*, *SLC47A1*, *SLC6A4*,
21 *CYP2C8*, and *CYP2C9*) were targets for 51 nervous system drugs¹⁰⁵ (anatomical
22 therapeutic chemical (ATC) codes starting with “N”), which was a higher probability of
23 overlap than by chance ($P = 0.027$). Specifically, there were 29 anti-depressants (N06A) to
24 treat MDD and related conditions, 13 anti-psychotics drugs (N05A) to manage psychosis,
25 4 psychostimulants (N06B) for attention-deficit/hyperactivity disorder (ADHD) and
26 nootropics, and 2 anti-migraine (N02C) (**Table S13**).
27

28 To identify brain cell types where genetic variation leads to changes in brain function, we
29 performed partitioned heritability analyses¹⁰⁶ for cell type-specific regulatory elements.
30 Specifically, we estimated partitioned heritability enrichment within differentially
31 accessible chromatin of neurons (NeuN+, including two subtypes GABAergic
32 [NeuN+/Sox6+] and glutamatergic neurons [NeuN+/Sox6-]) and glial cells (NeuN-,

1 including oligodendrocyte [NeuN-/Sox10+], microglia and astrocyte [NeuN-/Sox10-])¹⁰⁷.
2 To identify global enrichment across the whole brain, we performed partitioned
3 heritability using global functional connectivity and amplitude traits in resting fMRI. For
4 both functional connectivity and amplitude traits, there was a much stronger enrichment
5 in neuronal regulatory elements than in glia (Fig. 6A). For further resolution across brain
6 networks, we also performed enrichment analysis for the mean amplitude of the 12
7 networks. In most functional networks, neurons were more enriched than glia, and the
8 strongest neuronal enrichment was found in the posterior multimodal network (Fig. 6B).
9 These findings may indicate that common variants associated with brain functional
10 activity primarily affect the function of regulatory elements in neurons, which are
11 expected to influence brain functional interactions.

12

13 DISCUSSION

14 Most previous large-scale genetic studies of brain imaging data have focused on brain
15 structures. Nevertheless, brain functional traits could also connect genetic variations to
16 mechanisms underlying behavioral differences¹⁰⁸. Using resting and task fMRI data from
17 the UKB study, we provided fine details of genetic influences on cerebral cortex functional
18 architectures through a parcellation-based approach. We showed the similarities and
19 differences in the genetic architecture of intrinsic and extrinsic functional organizations.
20 Genetic colocalization and correlation analyses uncovered important brain functional
21 areas and networks that were genetically implicated in specific diseases and traits. Our
22 results may help guide future clinical research and applications in the field of
23 neurodegenerative and neuropsychiatric disorders. For example, structural MRI traits¹⁰⁹
24 (such as gray matter volumes) are frequently used as imaging biomarkers in practical
25 applications of Alzheimer's disease. However, we found substantial genetic links between
26 the visual cortex function and Alzheimer's disease, and there were stronger associations
27 with *APOE* ε4 in fMRI traits than in structural MRI traits. These findings suggest that fMRI
28 traits of the visual cortex may be used as endophenotypes of Alzheimer's disease.

29

30 At the group mean level, prior literature has demonstrated that the intrinsic and extrinsic
31 functional architectures are highly similar with small but consistent differences^{44,110-113}.
32 These task-related changes are essential for the human brain to adaptively alter its

1 functionality via rapid changes in inter-regional functional connectivity⁴⁴. Using large-
2 scale individual-level data, we showed the overall genetic similarity between resting and
3 task fMRI (e.g., mean genetic correlation = 0.7). Although the genetic differences between
4 resting and task fMRI may be small, several lines of evidence suggest such differences
5 could be important and are genetically related to cognition and brain diseases. For
6 example, cognitive function had genetic correlations with the secondary visual and
7 somatomotor networks during task performance, but not at rest.

8

9 Although many efforts have been made to understand the functional organizations of the
10 human brain, there is no one widely-accepted standard pipeline for functional
11 connectivity analysis in fMRI¹¹⁴. Our study is one of the first attempts to study the genetic
12 architecture of brain functions using a parcellation-based approach in a biobank-scale
13 dataset. The major difference between the whole brain ICA and parcellation-based
14 approaches is that the ICA regions are typically distributed across multiple regions and
15 different networks by combining their major variations. Compared to the recent whole
16 brain ICA-based studies^{31,33}, our parcellation-based approach was able to uncover high-
17 resolution fine details on the genetic effect patterns and enable the comparison between
18 intrinsic and extrinsic functional architectures. More importantly, our results suggest the
19 usefulness of specific fMRI phenotypes for different brain disorders from a genetic
20 perspective.

21

22 There are a few limitations in the present study. First, the UKB participants were mostly
23 middle-aged to elderly Europeans. Nonlinear aging effects on brain functional
24 connectivity have been widely observed¹¹⁵. We have used the ABCD study as a replication
25 dataset, it is of great interest to further study the gene-age interactions and evaluate the
26 generalizability of UKB results across the lifespan¹¹⁶. It is also interesting to investigate
27 the population-specific genetic components when more large-scale fMRI data from global
28 populations become available. Due to potentially different environmental influences and
29 population-specific genetic effects, fMRI traits could have different heritability across
30 ancestry groups. Second, the UKB task fMRI data were from a single emotion processing
31 task^{36,37}. Although previous studies have shown that the functional architectures of
32 different tasks were highly similar^{44,110,112}, multi-task fMRI data may provide new insights

1 in genetic studies. It might be possible to impute/predict multi-task fMRI data for UKB
2 using the multi-task HCP data as training reference panels. To allow comparison between
3 resting and task fMRI, our study focused on functional connectivity traits. It is also of great
4 interest to study genetics influences on task activation measures/maps for task fMRI.
5 Finally, this study partitioned the cerebral cortex using the Glasser360 atlas. By applying
6 more brain parcellations³ to the large-scale UKB dataset, it will be possible to establish
7 more useful imaging phenotypes for specific brain disorders.

8

9 **METHODS**

10 Methods are available in the **Methods** section.

11 *Note: One supplementary information pdf file, one supplementary figure pdf file, and one*
12 *supplementary table zip file are available.*

13

14 **ACKNOWLEDGEMENTS**

15 We thank Fidel Alfaro-Almagro and Doug Crabbill for their helpful conversations. The study
16 has been supported by start-up funds from Purdue Statistics Department and funding
17 from the Analytics at Wharton. This research was partially supported by U.S. NIH grants
18 MH086633 (HT.Z.) and MH116527 (TF.L. and HP.Z.). Assistance for this project was also
19 provided by the UNC Intellectual and Developmental Disabilities Research Center (NICHD;
20 P50 HD103573; Y.L.). We thank the individuals represented in the UK Biobank study for
21 their participation and the research teams for their work in collecting, processing, and
22 disseminating these datasets for analysis. We would like to thank the research computing
23 groups at the University of North Carolina at Chapel Hill, Purdue University, and the
24 Wharton School of the University of Pennsylvania for providing computational resources
25 and supports that have contributed to these research results. We gratefully acknowledge
26 all the studies and databases that made GWAS summary data available. This research has
27 been conducted using the UK Biobank resource (application number 22783), subject to a
28 data transfer agreement.

29

30 **AUTHOR CONTRIBUTIONS**

31 B.Z., HT.Z., J.L.S., and S.M.S. designed the study. B.Z., TF.L., Y.Y., X.Y., YL.Y., D.X., X.W., Z.Z.,
32 TY. L, Z.W., YJ.L., and Z.F. analyzed the data. TF. L., Z.Z., and Y.S. downloaded the datasets,

1 processed fMRI data, and undertook quantity controls. Y.L. and HP.Z. provided feedback
2 on the study design and results interpretation. B.Z. wrote the manuscript with feedback
3 from all authors.

4

5 **CORRESPONDENCE AND REQUESTS FOR MATERIALS** should be addressed to HT.Z.

6

7 **COMPETING FINANCIAL INTERESTS**

8 The authors declare no competing financial interests.

9

10 **REFERENCES**

- 11 1. Glasser, M.F. *et al.* A multi-modal parcellation of human cerebral cortex. *Nature*
12 **536**, 171-178 (2016).
- 13 2. Van Essen, D.C., Glasser, M.F., Dierker, D.L., Harwell, J. & Coalson, T.
14 Parcellations and hemispheric asymmetries of human cerebral cortex analyzed
15 on surface-based atlases. *Cerebral cortex* **22**, 2241-2262 (2012).
- 16 3. Eickhoff, S.B., Yeo, B.T. & Genon, S. Imaging-based parcellations of the human
17 brain. *Nature Reviews Neuroscience* **19**, 672-686 (2018).
- 18 4. Biswal, B., Zerrin Yetkin, F., Haughton, V.M. & Hyde, J.S. Functional connectivity
19 in the motor cortex of resting human brain using echo-planar MRI. *Magnetic*
20 *resonance in medicine* **34**, 537-541 (1995).
- 21 5. Belliveau, J. *et al.* Functional mapping of the human visual cortex by magnetic
22 resonance imaging. *Science* **254**, 716-719 (1991).
- 23 6. Mwansisya, T.E. *et al.* Task and resting-state fMRI studies in first-episode
24 schizophrenia: A systematic review. *Schizophrenia research* **189**, 9-18 (2017).
- 25 7. Xie, C. *et al.* A shared neural basis underlying psychiatric comorbidity. *Nature*
26 *medicine* **29**, 1232-1242 (2023).
- 27 8. Badhwar, A. *et al.* Resting-state network dysfunction in Alzheimer's disease: a
28 systematic review and meta-analysis. *Alzheimer's & Dementia: Diagnosis,*
29 *Assessment & Disease Monitoring* **8**, 73-85 (2017).
- 30 9. Wolters, A.F. *et al.* Resting-state fMRI in Parkinson's disease patients with
31 cognitive impairment: A meta-analysis. *Parkinsonism & Related Disorders* **62**, 16-
32 27 (2019).

- 1 10. Philip, R.C. *et al.* A systematic review and meta-analysis of the fMRI investigation
- 2 of autism spectrum disorders. *Neuroscience & Biobehavioral Reviews* **36**, 901-
- 3 942 (2012).
- 4 11. Mulders, P.C., van Eijndhoven, P.F., Schene, A.H., Beckmann, C.F. & Tendolkar, I.
- 5 Resting-state functional connectivity in major depressive disorder: a review.
- 6 *Neuroscience & Biobehavioral Reviews* **56**, 330-344 (2015).
- 7 12. Chen, D. *et al.* Neurophysiological stratification of major depressive disorder by
- 8 distinct trajectories. *Nature Mental Health*, 1-13 (2023).
- 9 13. Elliott, M.L. *et al.* What is the test-retest reliability of common task-functional
- 10 MRI measures? New empirical evidence and a meta-analysis. *Psychological*
- 11 *Science* **31**, 792-806 (2020).
- 12 14. Marek, S. *et al.* Towards reproducible brain-wide association studies. *BioRxiv*
- 13 (2020).
- 14 15. Smith, S.M. & Nichols, T.E. Statistical challenges in “big data” human
- 15 neuroimaging. *Neuron* **97**, 263-268 (2018).
- 16 16. Elliott, M.L. *et al.* General functional connectivity: Shared features of resting-
- 17 state and task fMRI drive reliable and heritable individual differences in
- 18 functional brain networks. *NeuroImage* **189**, 516-532 (2019).
- 19 17. Ge, T., Holmes, A.J., Buckner, R.L., Smoller, J.W. & Sabuncu, M.R. Heritability
- 20 analysis with repeat measurements and its application to resting-state functional
- 21 connectivity. *Proceedings of the National Academy of Sciences* **114**, 5521-5526
- 22 (2017).
- 23 18. Yang, Z. *et al.* Genetic and environmental contributions to functional
- 24 connectivity architecture of the human brain. *Cerebral cortex* **26**, 2341-2352
- 25 (2016).
- 26 19. Miranda-Dominguez, O. *et al.* Heritability of the human connectome: A
- 27 connectotyping study. *Network Neuroscience* **2**, 175-199 (2018).
- 28 20. Adhikari, B.M. *et al.* Heritability estimates on resting state fMRI data using
- 29 ENIGMA analysis pipeline. (2018).
- 30 21. Blokland, G.A. *et al.* Quantifying the heritability of task-related brain activation
- 31 and performance during the N-back working memory task: a twin fMRI study.
- 32 *Biological psychology* **79**, 70-79 (2008).

- 1 22. Colclough, G.L. *et al.* The heritability of multi-modal connectivity in human brain
- 2 activity. *Elife* **6**, e20178 (2017).
- 3 23. Teeuw, J. *et al.* Genetic and environmental influences on functional connectivity
- 4 within and between canonical cortical resting-state networks throughout
- 5 adolescent development in boys and girls. *Neuroimage* **202**, 116073 (2019).
- 6 24. Foo, H. *et al.* Genetic influence on ageing-related changes in resting-state brain
- 7 functional networks in healthy adults: a systematic review. *Neuroscience &*
- 8 *Biobehavioral Reviews* (2020).
- 9 25. Chaarani, B. *et al.* Baseline brain function in the preadolescents of the ABCD
- 10 Study. *Nature Neuroscience*, 1-11 (2021).
- 11 26. Miller, K.L. *et al.* Multimodal population brain imaging in the UK Biobank
- 12 prospective epidemiological study. *Nature Neuroscience* **19**, 1523-1536 (2016).
- 13 27. Littlejohns, T.J. *et al.* The UK Biobank imaging enhancement of 100,000
- 14 participants: rationale, data collection, management and future directions.
- 15 *Nature communications* **11**, 1-12 (2020).
- 16 28. Beckmann, C.F. & Smith, S.M. Probabilistic independent component analysis for
- 17 functional magnetic resonance imaging. *IEEE transactions on medical imaging*
- 18 **23**, 137-152 (2004).
- 19 29. Hyvarinen, A. Fast and robust fixed-point algorithms for independent component
- 20 analysis. *IEEE transactions on Neural Networks* **10**, 626-634 (1999).
- 21 30. Alfaro-Almagro, F. *et al.* Image processing and Quality Control for the first 10,000
- 22 brain imaging datasets from UK Biobank. *NeuroImage* **166**, 400-424 (2018).
- 23 31. Elliott, L.T. *et al.* Genome-wide association studies of brain imaging phenotypes
- 24 in UK Biobank. *Nature* **562**, 210-216 (2018).
- 25 32. Zhao, B. *et al.* Common variants contribute to intrinsic human brain functional
- 26 networks. *Nature Genetics* **in press** (2022).
- 27 33. Smith, S.M. *et al.* An expanded set of genome-wide association studies of brain
- 28 imaging phenotypes in UK Biobank. *Nature neuroscience* **24**, 737-745 (2021).
- 29 34. Lv, H. *et al.* Resting-state functional MRI: everything that nonexperts have always
- 30 wanted to know. *American Journal of Neuroradiology* **39**, 1390-1399 (2018).

- 1 35. Sudlow, C. *et al.* UK biobank: an open access resource for identifying the causes
2 of a wide range of complex diseases of middle and old age. *PLoS Medicine* **12**,
3 e1001779 (2015).
- 4 36. Hariri, A.R., Tessitore, A., Mattay, V.S., Fera, F. & Weinberger, D.R. The amygdala
5 response to emotional stimuli: a comparison of faces and scenes. *Neuroimage*
6 **17**, 317-323 (2002).
- 7 37. Barch, D.M. *et al.* Function in the human connectome: task-fMRI and individual
8 differences in behavior. *Neuroimage* **80**, 169-189 (2013).
- 9 38. Somerville, L.H. *et al.* The Lifespan Human Connectome Project in Development:
10 A large-scale study of brain connectivity development in 5–21 year olds.
Neuroimage **183**, 456-468 (2018).
- 12 39. Ji, J.L. *et al.* Mapping the human brain's cortical-subcortical functional network
13 organization. *Neuroimage* **185**, 35-57 (2019).
- 14 40. Bijsterbosch, J. *et al.* Investigations into within-and between-subject resting-
15 state amplitude variations. *Neuroimage* **159**, 57-69 (2017).
- 16 41. Yang, J., Lee, S.H., Goddard, M.E. & Visscher, P.M. GCTA: a tool for genome-wide
17 complex trait analysis. *The American Journal of Human Genetics* **88**, 76-82
18 (2011).
- 19 42. Türe, U., Yaşargil, D.C., Al-Mefty, O. & Yaşargil, M.G. Topographic anatomy of the
20 insular region. *Journal of neurosurgery* **90**, 720-733 (1999).
- 21 43. Nieuwenhuys, R. The insular cortex: a review. *Progress in brain research* **195**,
22 123-163 (2012).
- 23 44. Cole, M.W., Ito, T., Cocuzza, C. & Sanchez-Romero, R. The functional relevance of
24 task-state functional connectivity. *Journal of Neuroscience* **41**, 2684-2702 (2021).
- 25 45. Fox, M.D. & Raichle, M.E. Spontaneous fluctuations in brain activity observed
26 with functional magnetic resonance imaging. *Nature reviews neuroscience* **8**,
27 700-711 (2007).
- 28 46. Bulik-Sullivan, B.K. *et al.* LD Score regression distinguishes confounding from
29 polygenicity in genome-wide association studies. *Nature genetics* **47**, 291-295
30 (2015).

- 1 47. de Klein, N. *et al.* Brain expression quantitative trait locus and network analysis
2 reveals downstream effects and putative drivers for brain-related diseases.
3 *bioRxiv* (2021).
- 4 48. Hormozdiari, F. *et al.* Colocalization of GWAS and eQTL signals detects target
5 genes. *The American Journal of Human Genetics* **99**, 1245-1260 (2016).
- 6 49. Bulik-Sullivan, B. *et al.* An atlas of genetic correlations across human diseases
7 and traits. *Nature Genetics* **47**, 1236-1241 (2015).
- 8 50. Zhao, B. *et al.* Common genetic variation influencing human white matter
9 microstructure. *bioRxiv* (2020).
- 10 51. Yeo, B.T. *et al.* The organization of the human cerebral cortex estimated by
11 intrinsic functional connectivity. *Journal of neurophysiology* (2011).
- 12 52. Buniello, A. *et al.* The NHGRI-EBI GWAS Catalog of published genome-wide
13 association studies, targeted arrays and summary statistics 2019. *Nucleic Acids
14 Research* **47**, D1005-D1012 (2018).
- 15 53. Giambartolomei, C. *et al.* Bayesian test for colocalisation between pairs of
16 genetic association studies using summary statistics. *PLoS genetics* **10**, e1004383
17 (2014).
- 18 54. Kibinge, N.K., Relton, C.L., Gaunt, T.R. & Richardson, T.G. Characterizing the
19 causal pathway for genetic variants associated with neurological phenotypes
20 using human brain-derived proteome data. *The American Journal of Human
21 Genetics* **106**, 885-892 (2020).
- 22 55. Brewer, A.A. & Barton, B. Visual cortex in aging and Alzheimer's disease: changes
23 in visual field maps and population receptive fields. *Frontiers in psychology* **5**, 74
24 (2014).
- 25 56. Zhang, H.-Y. *et al.* Resting brain connectivity: changes during the progress of
26 Alzheimer disease. *Radiology* **256**, 598-606 (2010).
- 27 57. Wang, Z. *et al.* Functional connectivity changes across the spectrum of subjective
28 cognitive decline, amnestic mild cognitive impairment and Alzheimer's disease.
29 *Frontiers in neuroinformatics* **13**, 26 (2019).
- 30 58. Wink, A.M. *et al.* Functional brain network centrality is related to APOE genotype
31 in cognitively normal elderly. *Brain and behavior* **8**, e01080 (2018).

- 1 59. Dennis, E.L. & Thompson, P.M. Functional brain connectivity using fMRI in aging
- 2 and Alzheimer's disease. *Neuropsychology review* **24**, 49-62 (2014).
- 3 60. Palop, J.J. & Mucke, L. Network abnormalities and interneuron dysfunction in
- 4 Alzheimer disease. *Nature Reviews Neuroscience* **17**, 777-792 (2016).
- 5 61. Filippini, N. *et al.* Distinct patterns of brain activity in young carriers of the APOE-
- 6 ε4 allele. *Proceedings of the National Academy of Sciences* **106**, 7209-7214
- 7 (2009).
- 8 62. Palmqvist, S. *et al.* Earliest accumulation of β-amyloid occurs within the default-
- 9 mode network and concurrently affects brain connectivity. *Nature*
- 10 *communications* **8**, 1-13 (2017).
- 11 63. Zhao, B. *et al.* Genome-wide association analysis of 19,629 individuals identifies
- 12 variants influencing regional brain volumes and refines their genetic co-
- 13 architecture with cognitive and mental health traits. *Nature genetics* **51**, 1637-
- 14 1644 (2019).
- 15 64. Goes, F.S. *et al.* Genome-wide association study of schizophrenia in Ashkenazi
- 16 Jews. *American Journal of Medical Genetics Part B: Neuropsychiatric Genetics*
- 17 **168**, 649-659 (2015).
- 18 65. Li, Z. *et al.* Genome-wide association analysis identifies 30 new susceptibility loci
- 19 for schizophrenia. *Nature Genetics* **49**, 1576-1583 (2017).
- 20 66. Anney, R.J.L. *et al.* Meta-analysis of GWAS of over 16,000 individuals with autism
- 21 spectrum disorder highlights a novel locus at 10q24.32 and a significant overlap
- 22 with schizophrenia. *Molecular Autism* **8**, 21 (2017).
- 23 67. Hyde, C.L. *et al.* Identification of 15 genetic loci associated with risk of major
- 24 depression in individuals of European descent. *Nature genetics* **48**, 1031-1036
- 25 (2016).
- 26 68. Anney, R. *et al.* Genetic determinants of common epilepsies: a meta-analysis of
- 27 genome-wide association studies. *The Lancet Neurology* **13**, 893-903 (2014).
- 28 69. Lee, J.J. *et al.* Gene discovery and polygenic prediction from a genome-wide
- 29 association study of educational attainment in 1.1 million individuals. *Nature*
- 30 *Genetics* **50**, 1112–1121 (2018).
- 31 70. Kichaev, G. *et al.* Leveraging polygenic functional enrichment to improve GWAS
- 32 power. *The American Journal of Human Genetics* **104**, 65-75 (2019).

- 1 71. Baselmans, B.M. *et al.* Multivariate genome-wide analyses of the well-being
- 2 spectrum. *Nature genetics* **51**, 445-451 (2019).
- 3 72. Pickrell, J.K. *et al.* Detection and interpretation of shared genetic influences on
- 4 42 human traits. *Nature genetics* **48**, 709 (2016).
- 5 73. Anttila, V. *et al.* Genome-wide meta-analysis identifies new susceptibility loci for
- 6 migraine. *Nature genetics* **45**, 912 (2013).
- 7 74. Bakker, M.K. *et al.* Genome-wide association study of intracranial aneurysms
- 8 identifies 17 risk loci and genetic overlap with clinical risk factors. *Nature*
- 9 *genetics* **52**, 1303-1313 (2020).
- 10 75. Ikram, M.A. *et al.* Heritability and genome-wide associations studies of cerebral
- 11 blood flow in the general population. *Journal of Cerebral Blood Flow &*
- 12 *Metabolism* **38**, 1598-1608 (2018).
- 13 76. Skorobogatykh, K. *et al.* Functional connectivity studies in migraine: what have
- 14 we learned? *The journal of headache and pain* **20**, 1-10 (2019).
- 15 77. Savage, J.E. *et al.* Genome-wide association meta-analysis in 269,867 individuals
- 16 identifies new genetic and functional links to intelligence. *Nature Genetics* **50**,
- 17 912-919 (2018).
- 18 78. Gelernter, J. *et al.* Genome-wide association study of cocaine dependence and
- 19 related traits: FAM53B identified as a risk gene. *Molecular psychiatry* **19**, 717-
- 20 723 (2014).
- 21 79. Cavanna, A.E. & Trimble, M.R. The precuneus: a review of its functional anatomy
- 22 and behavioural correlates. *Brain* **129**, 564-583 (2006).
- 23 80. Cadwell, C.R., Bhaduri, A., Mostajo-Radji, M.A., Keefe, M.G. & Nowakowski, T.J.
- 24 Development and arealization of the cerebral cortex. *Neuron* **103**, 980-1004
- 25 (2019).
- 26 81. Nishikimi, M., Oishi, K., Tabata, H., Torii, K. & Nakajima, K. Segregation and
- 27 pathfinding of callosal axons through EphA3 signaling. *Journal of Neuroscience*
- 28 **31**, 16251-16260 (2011).
- 29 82. Jung, R.E. & Haier, R.J. The Parieto-Frontal Integration Theory (P-FIT) of
- 30 intelligence: converging neuroimaging evidence. *Behavioral and Brain Sciences*
- 31 **30**, 135 (2007).

- 1 83. Deary, I.J., Penke, L. & Johnson, W. The neuroscience of human intelligence
2 differences. *Nature reviews neuroscience* **11**, 201-211 (2010).
- 3 84. Linnér, R.K. *et al.* Genome-wide association analyses of risk tolerance and risky
4 behaviors in over 1 million individuals identify hundreds of loci and shared
5 genetic influences. *Nature Genetics* **51**, 245-257 (2019).
- 6 85. Floden, D., Alexander, M.P., Kubu, C., Katz, D. & Stuss, D.T. Impulsivity and risk-
7 taking behavior in focal frontal lobe lesions. *Neuropsychologia* **46**, 213-223
8 (2008).
- 9 86. Davies, G. *et al.* Study of 300,486 individuals identifies 148 independent genetic
10 loci influencing general cognitive function. *Nature Communications* **9**, 2098
11 (2018).
- 12 87. Pardiñas, A.F. *et al.* Common schizophrenia alleles are enriched in mutation-
13 intolerant genes and in regions under strong background selection. *Nature
14 Genetics* **50**, 381–389 (2018).
- 15 88. Consortium, C.-D.G.o.t.P.G. Identification of risk loci with shared effects on five
16 major psychiatric disorders: a genome-wide analysis. *The Lancet* **381**, 1371-1379
17 (2013).
- 18 89. Nagel, M., Watanabe, K., Stringer, S., Posthuma, D. & Van Der Sluis, S. Item-level
19 analyses reveal genetic heterogeneity in neuroticism. *Nature communications* **9**,
20 905 (2018).
- 21 90. de Leeuw, C.A., Mooij, J.M., Heskes, T. & Posthuma, D. MAGMA: generalized
22 gene-set analysis of GWAS data. *PLoS Computational Biology* **11**, e1004219
23 (2015).
- 24 91. Lek, M. *et al.* Analysis of protein-coding genetic variation in 60,706 humans.
25 *Nature* **536**, 285 (2016).
- 26 92. Walker, R.L. *et al.* Genetic Control of Expression and Splicing in Developing
27 Human Brain Informs Disease Mechanisms. *Cell* **179**, 750-771. e22 (2019).
- 28 93. Zhang, B. & Horvath, S. A General Framework for Weighted Gene Co-Expression
29 Network Analysis. *Statistical Applications in Genetics & Molecular Biology* **4**, 1-43
30 (2005).
- 31 94. Demers, C.H., Conley, E.D., Bogdan, R. & Hariri, A.R. Interactions between
32 anandamide and corticotropin-releasing factor signaling modulate human

- 1 amygdala function and risk for anxiety disorders: an imaging genetics strategy
2 for modeling molecular interactions. *Biological psychiatry* **80**, 356-362 (2016).

3 95. Pagliaccio, D. *et al.* HPA axis genetic variation, pubertal status, and sex interact
4 to predict amygdala and hippocampus responses to negative emotional faces in
5 school-age children. *Neuroimage* **109**, 1-11 (2015).

6 96. Pagliaccio, D. *et al.* Stress-system genes and life stress predict cortisol levels and
7 amygdala and hippocampal volumes in children. *Neuropsychopharmacology* **39**,
8 1245-1253 (2014).

9 97. Pagliaccio, D. *et al.* Amygdala functional connectivity, HPA axis genetic variation,
10 and life stress in children and relations to anxiety and emotion regulation.
11 *Journal of abnormal psychology* **124**, 817 (2015).

12 98. Vissers, L.E., Gilissen, C. & Veltman, J.A. Genetic studies in intellectual disability
13 and related disorders. *Nature Reviews Genetics* **17**, 9-18 (2016).

14 99. Lam, M. *et al.* Large-Scale Cognitive GWAS Meta-Analysis Reveals Tissue-Specific
15 Neural Expression and Potential Nootropic Drug Targets. *Cell reports* **21**, 2597-
16 2613 (2017).

17 100. Watanabe, K., Taskesen, E., Bochoven, A. & Posthuma, D. Functional mapping
18 and annotation of genetic associations with FUMA. *Nature Communications* **8**,
19 1826 (2017).

20 101. Morey, R.A. *et al.* Serotonin transporter gene polymorphisms and brain function
21 during emotional distraction from cognitive processing in posttraumatic stress
22 disorder. *BMC psychiatry* **11**, 1-13 (2011).

23 102. Provenzi, L., Giorda, R., Beri, S. & Montirosso, R. SLC6A4 methylation as an
24 epigenetic marker of life adversity exposures in humans: a systematic review of
25 literature. *Neuroscience & Biobehavioral Reviews* **71**, 7-20 (2016).

26 103. Swartz, J.R., Hariri, A.R. & Williamson, D.E. An epigenetic mechanism links
27 socioeconomic status to changes in depression-related brain function in high-risk
28 adolescents. *Molecular psychiatry* **22**, 209-214 (2017).

29 104. Pezawas, L. *et al.* Evidence of biologic epistasis between BDNF and SLC6A4 and
30 implications for depression. *Molecular psychiatry* **13**, 709-716 (2008).

- 1 105. Wang, Q. *et al.* A Bayesian framework that integrates multi-omics data and gene
- 2 networks predicts risk genes from schizophrenia GWAS data. *Nature neuroscience* **22**, 691 (2019).
- 3
- 4 106. Finucane, H.K. *et al.* Partitioning heritability by functional annotation using
- 5 genome-wide association summary statistics. *Nature genetics* **47**, 1228-1235
- 6 (2015).
- 7 107. Hauberg, M.E. *et al.* Common schizophrenia risk variants are enriched in open
- 8 chromatin regions of human glutamatergic neurons. *Nature communications* **11**, 1-16 (2020).
- 9
- 10 108. Matoba, N. & Stein, J.L. From base pair to brain. *Nature Neuroscience* **24**, 619-
- 11 621 (2021).
- 12
- 13 109. Hansson, O. Biomarkers for neurodegenerative diseases. *Nature Medicine* **27**, 954-963 (2021).
- 14
- 15 110. Cole, M.W., Bassett, D.S., Power, J.D., Braver, T.S. & Petersen, S.E. Intrinsic and
- 16 task-evoked network architectures of the human brain. *Neuron* **83**, 238-251
- 17 (2014).
- 18
- 19 111. Tavor, I. *et al.* Task-free MRI predicts individual differences in brain activity
- 20 during task performance. *Science* **352**, 216-220 (2016).
- 21
- 22 112. Gonzalez-Castillo, J. & Bandettini, P.A. Task-based dynamic functional
- 23 connectivity: Recent findings and open questions. *Neuroimage* **180**, 526-533
- 24 (2018).
- 25
- 26 113. Gratton, C. *et al.* Functional brain networks are dominated by stable group and
- 27 individual factors, not cognitive or daily variation. *Neuron* **98**, 439-452. e5 (2018).
- 28
- 29 114. Pervaiz, U., Vidaurre, D., Woolrich, M.W. & Smith, S.M. Optimising network
- 30 modelling methods for fMRI. *Neuroimage* **211**, 116604 (2020).
- 31
- 32 115. Dosenbach, N.U. *et al.* Prediction of individual brain maturity using fMRI. *Science* **329**, 1358-1361 (2010).
- 33
- 34 116. Betzel, R.F. *et al.* Changes in structural and functional connectivity among
- 35 resting-state networks across the human lifespan. *Neuroimage* **102**, 345-357
- 36 (2014).
- 37
- 38 117. Dickie, E.W. *et al.* Ciftify: A framework for surface-based analysis of legacy MR
- 39 acquisitions. *Neuroimage* **197**, 818-826 (2019).

- 1 118. Rolls, E.T., Huang, C.-C., Lin, C.-P., Feng, J. & Joliot, M. Automated anatomical
- 2 labelling atlas 3. *NeuroImage* **206**, 116189 (2020).
- 3 119. Bycroft, C. *et al.* The UK Biobank resource with deep phenotyping and genomic
- 4 data. *Nature* **562**, 203-209 (2018).
- 5 120. Jiang, L. *et al.* A resource-efficient tool for mixed model association analysis of
- 6 large-scale data. *Nature genetics* **51**, 1749 (2019).
- 7 121. Purcell, S. *et al.* PLINK: a tool set for whole-genome association and population-
- 8 based linkage analyses. *The American Journal of Human Genetics* **81**, 559-575
- 9 (2007).

10

11 METHODS

12 **Imaging datasets.** We used the raw resting and task fMRI data from the UKB study, as
13 well as raw resting fMRI data from the ABCD study. The UKB study obtained ethics
14 approval from the North West Multicentre Research Ethics Committee (approval number:
15 11/NW/0382). All procedures in the ABCD study were approved by the institutional
16 review boards at ABCD collection sites (approval numbers: 201708123 and 160091). The
17 image acquisition and preprocessing procedures were detailed in the **Supplementary**
18 **Note.** The UKB task fMRI study implemented the emotion processing task^{36,37}. In this
19 study, the time series were extracted from the whole scan of the task fMRI data (including
20 blocks of both Shape and Face activations, Data-Category 106). Thus, all contrasts were
21 analyzed together when we calculated the functional connectivity measurements in
22 downstream analysis. We used a parcellation-based approach based on the Glasser360
23 atlas¹. Briefly, for each subject, we projected the resting and task fMRI data onto the
24 Glasser360 atlas and obtained the 360×360 functional connectivity matrices. The original
25 Glasser360 atlas is a surface-based parcellation for the cerebral cortex¹¹⁷ and it has been
26 transformed into a volumetric atlas that is compatible with the UKB volume-based data
27 (**Supplementary Note**). The 360 functional areas were grouped into 12 functional
28 networks³⁹ (**Table S1**). To aid interpretation, the 360 functional areas were labeled using
29 the automated anatomical labeling atlas¹¹⁸. We examined the spatial overlaps between
30 the Glasser360 functional areas and the whole brain ICA-defined brain regions generated
31 from the previous 25-dimension and 100-dimensions ICA analyses³⁰ (**Figs. 1B** and **S2**).

32

1 We mainly studied two sets of fMRI traits: area-level traits and network-level traits. Area-
2 level traits were the 8,531 functional connectivity measurements among all area pairs
3 within each of the 12 networks, which provided fine details on cerebral cortex functional
4 organizations and enabled the comparison between intrinsic and extrinsic functional
5 architectures. Network-level traits were expected to aggregate the major information
6 from the area-level traits. We input area-level functional connectivity traits and extracted
7 their low-rank representations/phenotypes via a combined PCA and ICA²⁹ dimension
8 reduction approach in a training-validation design³¹. The low-rank imaging phenotypes
9 were linear combinations of area-level traits and were independent of each other. We
10 used a training-validation design (across two sets of independent subjects) to optimize
11 both the initial dimensionality in the PCA step and the final number of ICA components
12 (with the reproducibility of ICA weight vectors > 0.9). Specifically, the Glasser360 atlas
13 classified 360 functional areas (nodes) into 12 networks, resulting in $360 \times 359/2 = 64,620$
14 functional connectivity traits between all pairs of functional areas (edges). The 12
15 networks allowed for categorizing all edges into 78 network-based groups, including 12
16 within-network groups, such as the default mode group, where both nodes of the edge
17 were in the default mode network. There were 66 between-network groups, such as the
18 sensorimotor-default mode group, where the two nodes of an edge came from
19 sensorimotor and default mode networks, respectively. The top ICA components were
20 extracted from each of the 78 network-based groups, which were interpreted as the
21 network-level functional connectivity traits. These ICA components have been mapped
22 back to the 360 functional areas of the Glasser360 atlas and visualizations have been
23 provided to facilitate biological interpretations (Fig. S78). Additionally, we considered the
24 mean amplitude of each network (12 networks in total), which was a measure of brain
25 activity⁴⁰. The network-level feature extraction was performed separately for resting and
26 task fMRI. Together, there were 1,985 network-level traits, 1,066 of which were from
27 resting fMRI and 919 from task fMRI. Detailed steps of our parcellation-based dimension
28 reduction procedure can be found in the **Supplementary Note** and the overview of the
29 procedure and study design can be found in **Figure S1**. Overall, the network-level
30 amplitude traits described the average brain activity across all brain functional areas
31 within the network; and the network-level functional connectivity traits quantified the

1 strength of functional connectivity within each network or between two different
2 networks.

3

4 We analyzed the following datasets separately: 1) the white British discovery GWAS,
5 which used data of individuals of white British ancestry in UKB phases 1 to 3 data ($n =$
6 34,641 for resting and 32,144 for task, released up through 2020); 2) European validation
7 GWAS: UKB white but non-British individuals in phases 1 to 3 data and all White
8 individuals in newly released UKB phases 4 and 5 data (UKBW, $n = 8,197$ for resting and
9 7,684 for task); 3) two non-European UKB validation GWAS: UKB Asian (UKBA, $n = 517$ for
10 resting and 429 for task) and UKB Black (UKBBL, $n = 283$ for resting and 231 for task); and
11 4) the UKB first revisit data ($n = 1,491$ for resting and 1,362 for task). The average age (at
12 imaging) of all subjects was 64.16 (standard error = 7.73), 51.6% were females. The
13 assignment of ancestry in UKB was based on self-reported ethnicity (Data-Field 21000),
14 which was verified in Bycroft, et al.¹¹⁹. We have also used the resting fMRI data from the
15 ABCD study as non-UKB replication datasets ($n = 3,821$ for European, 768 for Hispanic,
16 and 1,257 for African American cohorts). Details of ABCD data processing can be found in
17 **Supplementary Note**.

18

19 **Heritability and GWAS analysis.** We downloaded the imputed data from UKB data
20 resources¹¹⁹ (Data-Category 263). We performed the following quality controls on
21 subjects with both imaging and genetics data: 1) excluded subjects with more than 10%
22 missing genotypes; 2) excluded variants with minor allele frequency less than 0.01; 3)
23 excluded variants with missing genotype rate larger than 10%; 4) excluded variants that
24 failed the Hardy-Weinberg test at 1×10^{-7} level; and 5) removed variants with imputation
25 INFO score less than 0.8. SNP heritability was estimated by GCTA⁴¹ using all autosomal
26 SNPs in the white British discovery GWAS. We adjusted the effects of age (at imaging),
27 age-squared, sex, age-sex interaction, age-squared-sex interaction, imaging site, the top
28 40 genetic principal components (PCs)¹¹⁹, as well as the head motion, head motion-
29 squared, brain position, brain position-squared, and volumetric scaling. We also
30 examined the genetic variance estimates from the GCTA. Genome-wide association
31 analysis was performed in linear mixed effect models using fastGWA¹²⁰, while adjusting
32 the same set of covariates as in GCTA. GWAS were also separately performed via Plink¹²¹

1 in validation datasets, where we adjusted for the top ten genetic PCs instead of the top
2 40. We removed values greater than five times the median absolute deviation from the
3 median for each continuous phenotype or covariate variable. For area-level traits, the
4 independent lead variants were clumped by Plink ($LD\ r^2 < 0.1$, --clump-r2 0.1 --clump-kb
5 250). The genomic loci associated with network-level traits were defined using FUMA¹⁰⁰
6 (version 1.3.5e). Specifically, to define the LD boundaries, FUMA identified independent
7 significant variants, which were defined as variants with a *P*-value smaller than the
8 predefined threshold and were independent of other significant variants ($LD\ r^2 < 0.6$).
9 FUMA then constructed LD blocks for these independent significant variants by tagging
10 all variants in LD ($r^2 \geq 0.6$) with at least one independent significant variant and had a MAF
11 ≥ 0.0005 . These variants included those from the 1000 Genomes reference panel that
12 may not have been included in the GWAS. Moreover, within these significant variants,
13 independent lead variants were identified as those that were independent of each other
14 ($LD\ r^2 < 0.1$). If LD blocks of independent significant variants were close (< 250 kb based
15 on the closest boundary variants of LD blocks), they were merged into a single genomic
16 locus. Thus, each genomic locus could contain multiple significant variants and lead
17 variants. Independent significant variants and all the variants in LD with them ($r^2 \geq 0.6$)
18 were searched on the NHGRI-EBI GWAS catalog (version 2019-09-24) to look for
19 previously reported associations ($P < 9 \times 10^{-6}$) with any traits. We performed association
20 analysis to illustrate association patterns for selected colocalized index variants across all
21 64,620 functional connectivity traits in resting and task fMRI. The significance threshold
22 was set to be 3.86×10^{-7} ($0.05/(64,620 \times 2)$). The same set of covariates used in the above
23 GWAS analysis was adjusted in this analysis. LDSC⁴⁹ (version 1.0.1) was used to estimate
24 and test genetic correlations. We used the pre-calculated LD scores provided by LDSC,
25 which were computed using 1000 Genomes European data. We used HapMap3 variants
26 and removed all variants in the major histocompatibility complex (MHC) region.
27
28 We performed several additional heritability and GWAS analyses. First, we used the Yeo-
29 7 atlas⁵¹ to categorize the 360 Glasser areas into 7 functional networks. We applied the
30 same dimension reduction procedure as we used for the 12 functional networks³⁹, and
31 generated 615 network-level traits (294 for resting and 321 for task). Using the same set
32 of covariates as we used in the main analysis, we performed SNP heritability and GWAS

1 analyses for these Yeo-7 network-level traits. Second, we implemented additional quality
2 control procedures to remove potentially poor-quality images. After these additional
3 quality controls, we rerun our heritability and GWAS analyses to examine the robustness
4 of the results reported in our main analyses. Details of the Yeo-7 traits generation and
5 additional quality controls can be found in the **Supplementary Note**. Furthermore, we
6 split our discovery GWAS sample into two independent parts and performed GWAS
7 separately to evaluate genetic effect estimates in two datasets with equal sample sizes
8 and homogenous genetic backgrounds.

9

10 **Gene-level analysis and biological annotation.** Gene-based association analysis was
11 performed in UKB white British discovery GWAS for 18,796 protein-coding genes using
12 MAGMA⁹⁰ (version 1.08). Default MAGMA settings were used with zero window size
13 around each gene. We then carried out FUMA functional annotation and mapping
14 analysis, in which variants were annotated with their biological functionality and then
15 were linked to 35,808 candidate genes by a combination of positional, eQTL, and 3D
16 chromatin interaction mappings. Brain-related tissues/cells were selected in all options
17 and the default values were used for all other parameters in FUMA. We also explored the
18 overlaps with drug target genes using a nervous system drug target database¹⁰⁵, which
19 contained 241 target genes for 273 nervous system drugs. We tested for whether the
20 number of overlapping genes was greater than the expected number by chance using the
21 Chi-squared test with the resampling-based *P*-value. We performed heritability
22 enrichment analysis via partitioned LDSC¹⁰⁶. Baseline models were adjusted when
23 estimating and testing the enrichment scores for our brain cell type-specific annotations.

24

25 **Code availability**

26 We made use of publicly available software and tools. The codes used in fMRI
27 preprocessing and the parcellation-based network-level feature extraction pipeline will
28 be shared on Zenodo.

29

30 **Data availability**

31 The individual-level data used in the present study can be applied from the UK Biobank
32 (<https://www.ukbiobank.ac.uk/>) and ABCD (<https://abcdstudy.org/>) studies. Our GWAS

1 summary statistics will be shared on Zenodo and BIG-KP <https://bigkp.org/>. 3D
2 visualizations of ICA components can be downloaded at:
3 https://www.dropbox.com/s/np0rjlzvfa4fgae/Resting_fMRI_ICA.zip?dl=0 (for resting
4 fMRI) and https://www.dropbox.com/s/rg053royl62z12v/Task_fMRI_ICA.zip?dl=0 (for
5 task fMRI).

6

7 **Fig. 1 Illustration of the parcellation-based brain areas in the Glasser360 atlas and the**
8 **comparison with selected whole brain ICA-defined brain regions.**

9 **(A)** We illustrate the 360 functional areas and 12 networks defined in the Glasser360 atlas.
10 We generated functional connectivity traits based on these brain areas in both resting
11 and task fMRI to investigate genetic influences on brain function. Table S1 provides
12 information on these Glasser360 areas. Visual1, the primary visual network; Visual2, the
13 secondary visual network. **(B)** We illustrate the spatial overlaps between the Glasser360
14 atlas and two selected whole brain ICA-defined brain regions (Net100_Node5 and
15 Net100_Node44 in the left and right panels, respectively). The two ICA regions were
16 previously generated from a 100-dimensions ICA analysis³⁰ and estimated to have a high
17 level of heritability³². Here we show that these two ICA regions distribute across multiple
18 brain areas and networks in the Glasser360 atlas, as highlighted by dots with names being
19 labeled. Specifically, the Net100_Node5 region (mainly in the precuneus, angular, middle
20 cingulate) overlapped with 20 areas in the default mode, frontoparietal, and language
21 networks, and the Net100_Node44 region (mainly in the inferior frontal) overlapped with
22 21 areas in the frontoparietal, language, cingulo-opercular, and default mode networks.
23 A summary of such overlaps and additional examples of ICA regions can be found in Figure
24 S2.

25

26 **Fig. 2 SNP heritability pattern in resting and task fMRI.**

27 **(A)** The dots represent the SNP heritability estimates of fMRI traits, including 8,531 area-
28 level and 1,066 network-level traits in resting fMRI (left panel), and 8,531 area-level traits
29 and 919 network-level traits in task fMRI (right panel). The dots with gray color represent
30 non-significant heritability estimates (after controlling for multiple testing at a false
31 discovery rate of 5%). The mean heritability of each group is labeled, for example, the

1 mean heritability of traits in the auditory network was 14.5% in resting fMRI. **(B)**
2 Significant SNP heritability estimates of the functional connectivity traits within the
3 default mode network in resting fMRI (white dots are insignificant estimates). We
4 grouped all brain areas of the default mode network into seven clusters, which were
5 mainly organized by their physical locations (Fig. S7). OFC, orbitofrontal complex. The x
6 and y axis represent the names of the brain areas. **(C)** Comparison of SNP heritability
7 between the activated areas (within the activation, defined by the Shapes activation in
8 task fMRI) and the nonactivated areas (out activation) in resting fMRI (upper panel) and
9 task fMRI (lower panel). More information about the Shapes activation is available in
10 Alfaro-Almagro, et al. ³⁰.

11

12 **Fig. 3 The associated genomic regions of fMRI traits.**

13 **(A)** Ideogram of 47 genomic regions influencing fMRI traits, with 32 regions identified by
14 area-level traits ($P < 2.93 \times 10^{-12}$) and 15 more identified by network-level traits ($P < 2.51$
15 $\times 10^{-11}$). Each dot represents a genomic region, and the colors correspond to the 12
16 networks (and their interactions, named Between networks). A signal dot indicates that
17 at least one fMRI trait (either area- or network-level) of the corresponding network is
18 associated with the genomic region. Red and brown labels indicate genomic regions that
19 were replicated at the Bonferroni significance level and nominal significance level,
20 respectively. **(B)** The 19q13.32 genomic region was found to be associated with several
21 functional areas ($P < 2.93 \times 10^{-12}$), most of which were in the secondary visual network.
22 The colors of the brain areas represent different networks, and significant brain areas are
23 highlighted with red labels.

24

25 **Fig. 4 Genetic locus associated with both fMRI traits and Alzheimer's disease.**

26 In the 19q13.32 region, the *APOE* ε4 locus (index variant rs429358) showed associations
27 with both Alzheimer's disease and functional connectivity measurements. In **(A)**, we
28 illustrate the shared genetic influences for one functional connectivity trait of the default
29 mode network (Default <-> Default) in resting fMRI. In **(B)**, we illustrate the shared genetic
30 influences for one functional connectivity trait of the secondary visual network (Visual 2

1 <-> Visual 2) in task fMRI. In **(C)**, we illustrate the *P*-value of associations between the
2 rs429358 and various neuroimaging traits, including functional connectivity traits in
3 resting fMRI, functional connectivity traits in task fMRI, as well as structural traits (in gray
4 color), including diffusion tensor imaging (DTI) traits from diffusion MRI and regional brain
5 volumes from structural MRI. The strongest genetic effects were observed in the
6 secondary visual network for both resting and task fMRI.

7

8 **Fig. 5 Selected pairwise genetic correlations between fMRI traits and cognitive function**
9 **and schizophrenia.**

10 **(A)** We illustrate significant genetic correlations between cognitive function and
11 functional connectivity across different networks in resting fMRI at the FDR 5% level.
12 These significant genetic correlations were particularly related to functional connectivity
13 traits of specific areas, including the right IFSa in the cingulo-opercular network. Most of
14 the genetic correlations were negative. See Table S10 for the full list of estimates. **(B)** We
15 illustrate significant genetic correlations between schizophrenia and functional
16 connectivity across different networks in resting fMRI at the FDR 5% level. These
17 significant genetic correlations were particularly related to the functional connectivity
18 traits of specific areas, including the left 47s in the default mode network and the right
19 LIPv in the secondary visual network. **(C)** We illustrate significant genetic correlations
20 between cognitive function and functional connectivity across different networks in task
21 fMRI at the FDR 5% level. These significant genetic correlations were particularly related
22 to the functional connectivity traits of specific areas, including the left POS1 in the default
23 mode network and the right V6 in the secondary visual network. Similar to the resting
24 fMRI results in (A), genetic correlations of cognitive function with the default mode and
25 dorsal attention networks were negative in task fMRI. However, the genetic correlations
26 of cognitive function with the cingulo-opercular network became positive, and the
27 somatomotor and secondary visual networks also had positive genetic correlations in task
28 fMRI.

29

30 **Fig. 6 Partitioned heritability enrichment analysis.**

1 **(A)** Heritability enrichment of global functional connectivity and global amplitude of
2 resting fMRI in regulatory elements of glial cells (glia, including all glial cells,
3 oligodendrocyte subtype, and microglia/astrocyte subtype) and neuronal cells (neurons,
4 including all neurons, GABAergic subtype, and glutamatergic subtype). The dashed lines
5 indicate the nominal significance level. **(B)** Heritability enrichment of mean amplitude of
6 the 12 functional networks in regulatory elements of glial and neuronal cell types.

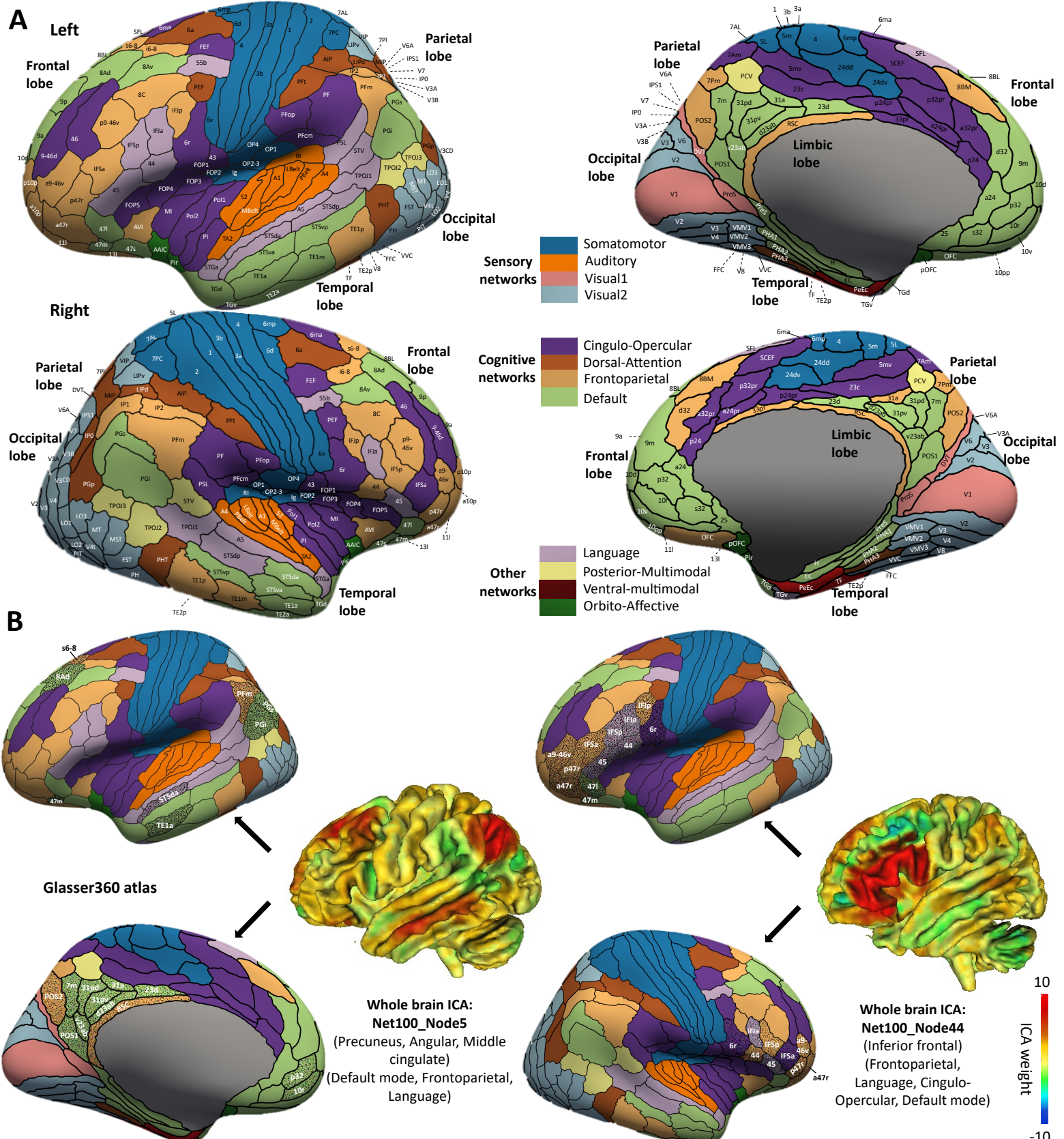


Figure 1

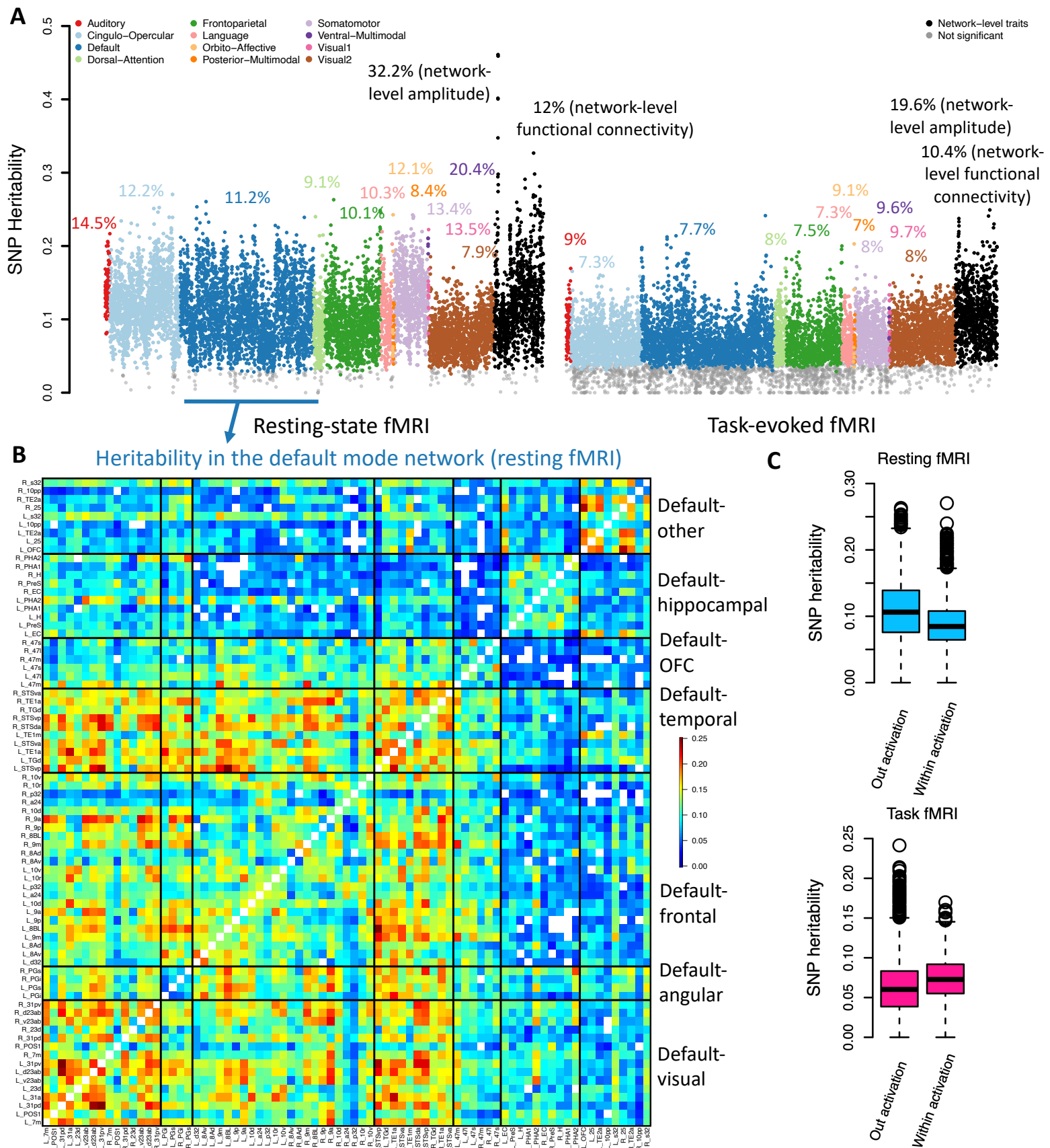


Figure 2

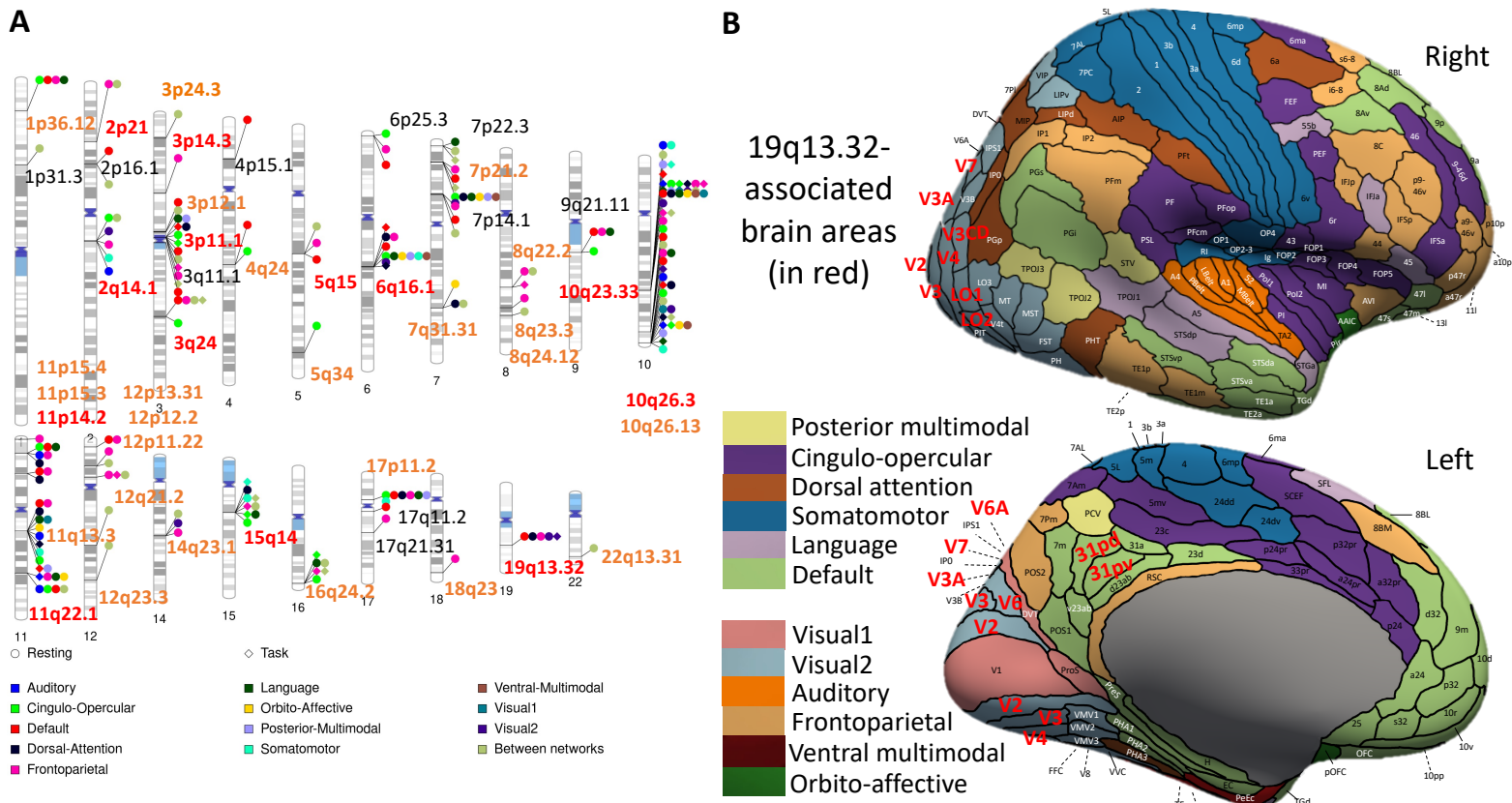
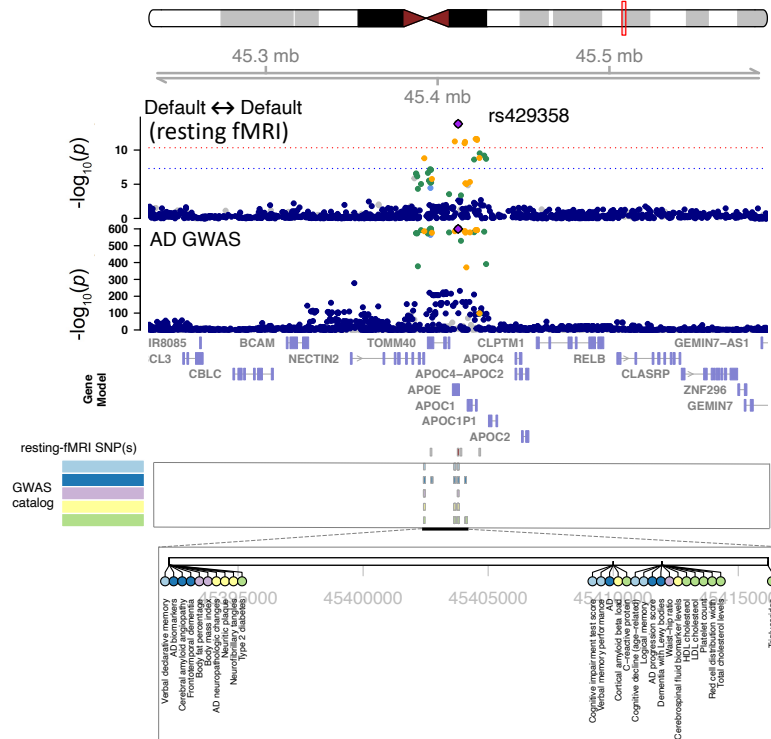


Figure 3

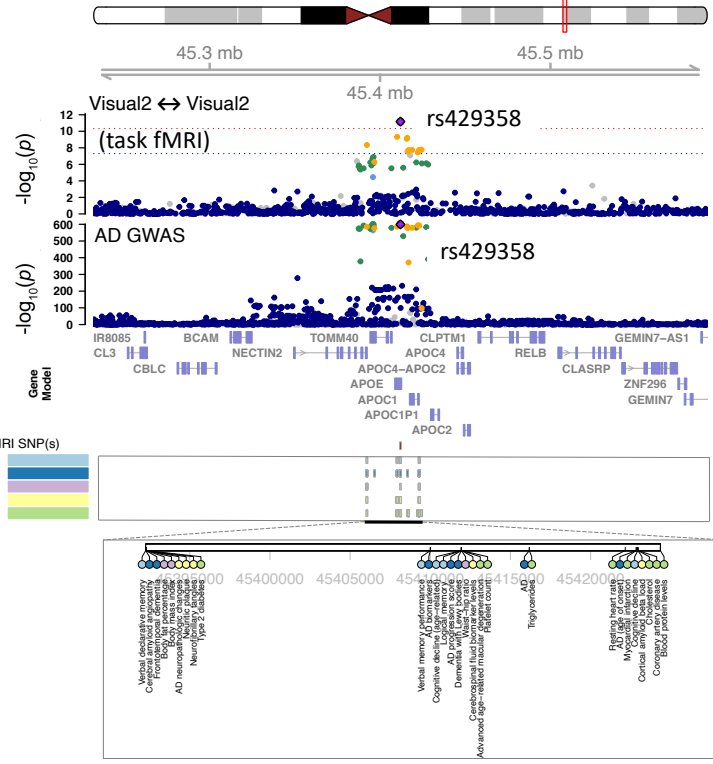
A

chr19, Region: 19q13.32



B

chr19, Region: 19q13.32



C

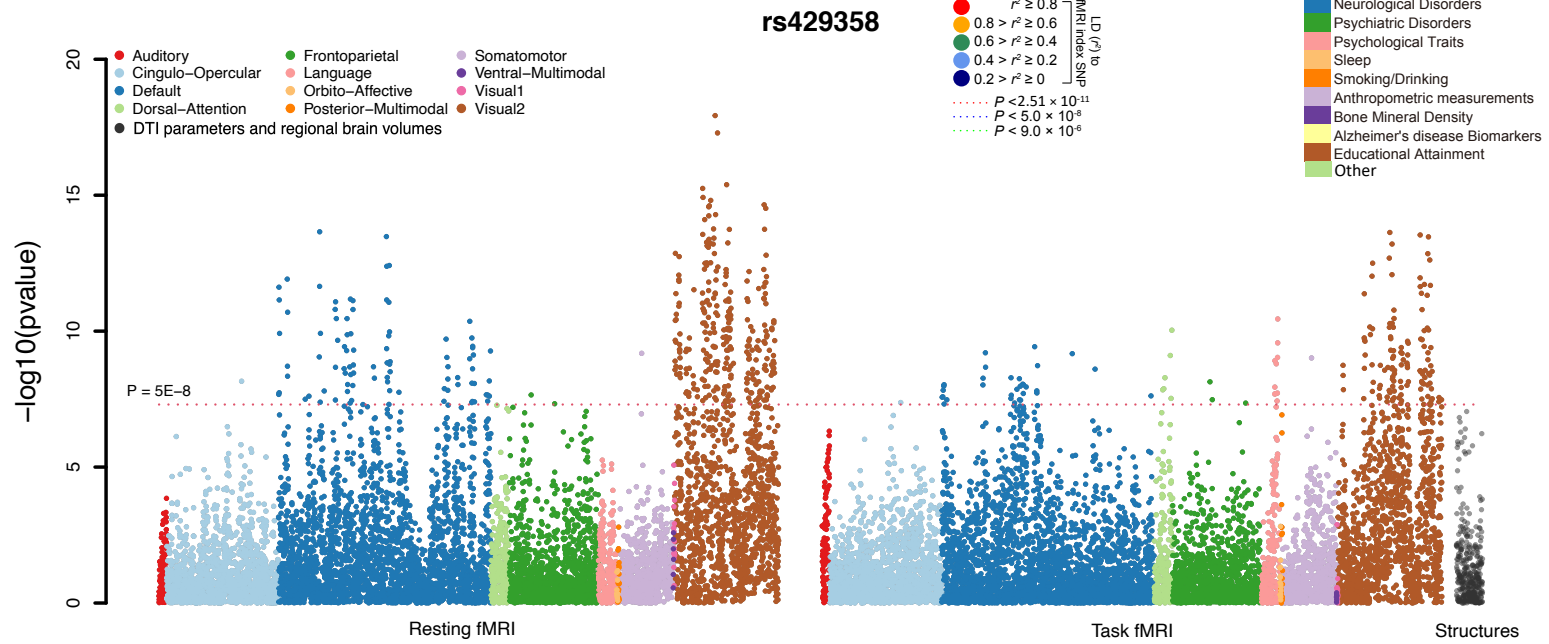


Figure 4

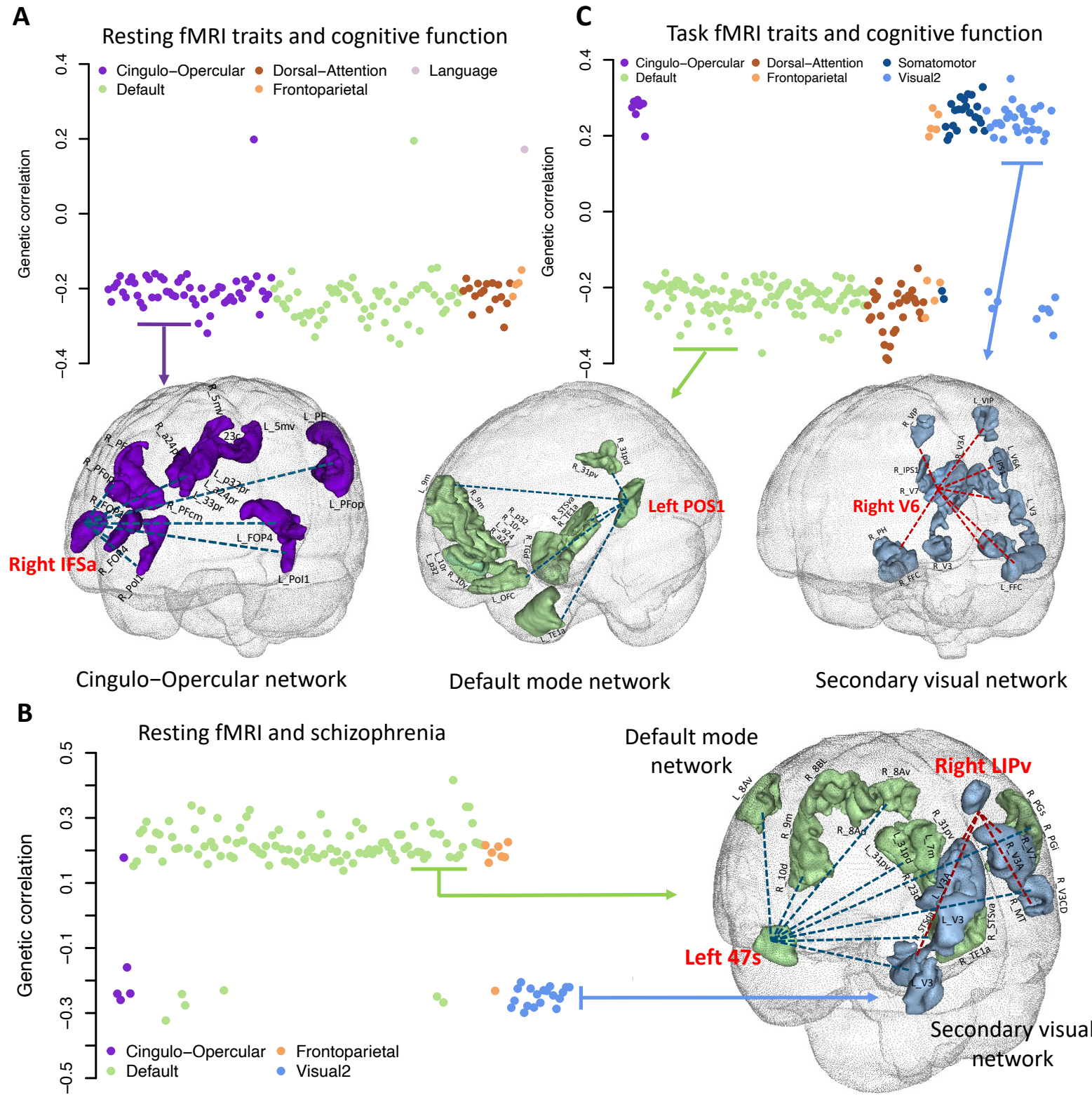


Figure 5

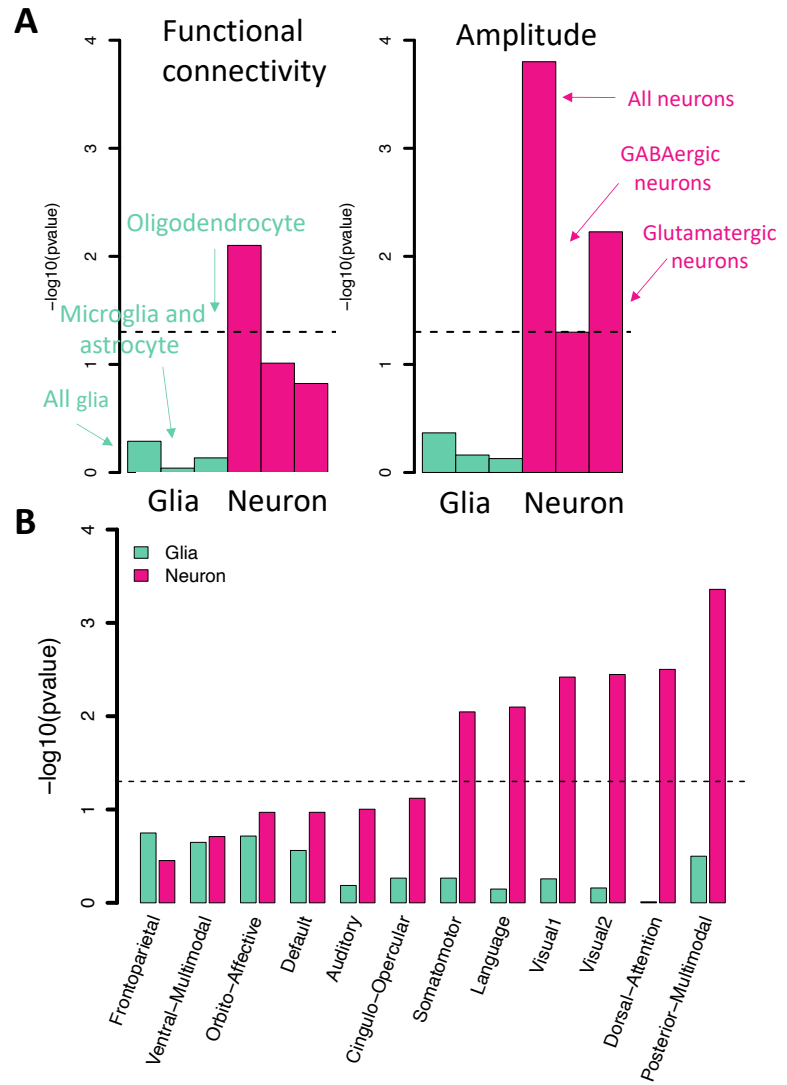


Figure 6